Journal for ImmunoTherapy of Cancer

# Vectorized Treg-depleting αCTLA-4 elicits antigen cross-presentation and CD8$^+$ T cell immunity to reject 'cold' tumors

Monika Semmrich,[1] Jean-Baptiste Marchand,[2] Laetitia Fend,[2] Matilda Rehn,[1] Christelle Remy,[2] Petra Holmkvist,[1] Nathalie Silvestre,[2] Carolin Svensson,[1] Patricia Kleinpeter,[2] Jules Deforges,[2] Fred Junghus,[1] Kirstie L Cleary,[3] Mimoza Bodén,[1] Linda Mårtensson,[1] Johann Foloppe,[2] Ingrid Teige,[1] Eric Quéméneur,[2] Björn Frendéus [1,3]

**To cite:** Semmrich M, Marchand J-B, Fend L, *et al*. Vectorized Treg-depleting αCTLA-4 elicits antigen cross-presentation and CD8$^+$ T cell immunity to reject 'cold' tumors. *Journal for ImmunoTherapy of Cancer* 2022;**10**:e003488. doi:10.1136/jitc-2021-003488

► Additional supplemental material is published online only. To view, please visit the journal online (http://dx.doi.org/10.1136/jitc-2021-003488).

MS and J-BM are joint first authors.

EQ and BF are joint senior authors.

Accepted 27 December 2021

Check for updates

© Author(s) (or their employer(s)) 2022. Re-use permitted under CC BY-NC. No commercial re-use. See rights and permissions. Published by BMJ.

For numbered affiliations see end of article.

**Correspondence to**
Dr Björn Frendéus;
bjorn.frendeus@bioinvent.com

## ABSTRACT

**Background** Immune checkpoint blockade (ICB) is a clinically proven concept to treat cancer. Still, a majority of patients with cancer including those with poorly immune infiltrated 'cold' tumors are resistant to currently available ICB therapies. Cytotoxic T lymphocyte-associated antigen-4 (CTLA-4) is one of few clinically validated targets for ICB, but toxicities linked to efficacy in approved αCTLA-4 regimens have restricted their use and precluded full therapeutic dosing. At a mechanistic level, accumulating preclinical and clinical data indicate dual mechanisms for αCTLA-4; ICB and regulatory T cell (Treg) depletion are both thought to contribute efficacy and toxicity in available, systemic, αCTLA-4 regimens. Accordingly, strategies to deliver highly effective, yet safe αCTLA-4 therapies have been lacking. Here we assess and identify spatially restricted exposure to a novel strongly Treg-depleting, checkpoint-blocking, vectorized αCTLA-4, as a highly efficacious and potentially safe strategy to target CTLA-4.

**Methods** A novel human IgG1 CTLA-4 antibody (4-E03) was identified using function-first screening for monoclonal antibodies (mAbs) and targets associated with superior Treg-depleting activity. A tumor-selective oncolytic vaccinia vector was then engineered to encode this novel, strongly Treg-depleting, checkpoint-blocking, αCTLA-4 antibody or a matching surrogate antibody, and Granulocyte-macrophage colony-stimulating factor (GM-CSF) ($VV_{GM}$-αCTLA-4).

**Results** The identified 4-E03 antibody showed significantly stronger Treg depletion, but equipotent checkpoint blockade, compared with clinically validated αCTLA-4 ipilimumab against CTLA-4-expressing Treg cells in a humanized mouse model in vivo. Intratumoral administration of $VV_{GM}$-αCTLA-4 achieved tumor-restricted CTLA-4 receptor saturation and Treg depletion, which elicited antigen cross-presentation and stronger systemic expansion of tumor-specific CD8$^+$ T cells and antitumor immunity compared with systemic αCTLA-4 antibody therapy. Efficacy correlated with FcγR-mediated intratumoral Treg depletion. Remarkably, in a clinically relevant mouse model resistant to systemic ICB, intratumoral $VV_{GM}$-αCTLA-4 synergized with αPD-1 to reject cold tumors.

**Conclusion** Our findings demonstrate in vivo proof of concept for spatial restriction of Treg depletion-optimized immune checkpoint blocking, vectorized αCTLA-4 as a highly effective and safe strategy to target CTLA-4. A clinical trial evaluating intratumoral $VV_{GM}$-αhCTLA-4 (BT-001) alone and in combination with αPD-1 in metastatic or advanced solid tumors has commenced.

## INTRODUCTION

Treatment with immune checkpoint blocking antibodies has transformed survival of patients with advanced solid cancers including metastatic melanoma, non-small cell lung cancer and mismatch repair-deficient cancers.[1–3] Still, a great unmet need remains since many patients fail to respond or acquire resistance to immune checkpoint blockade (ICB).[4] Reasons for lack of efficacy are believed to include lack of, or inadequate, tumor-infiltrating lymphocytes (TILs), most notably CD8$^+$ T cells.[5 6] Paucity of chemotactic and inflammatory signals in the solid cancer tumor microenvironment (TME) is similarly thought to underlie resistance to chimeric antigen receptor (CAR) T cell therapy.[7]

Identification of therapeutics that induce recruitment of inflammatory immune cells into 'immune desert' or 'immune-excluded' tumors, translating into robust systemic adaptive antitumor immunity and CD8$^+$ T cell infiltration with regression of primary and metastasized tumors, is therefore highly desired.

Intratumoral oncolytic virotherapy induces T cell infiltration and improves αPD-1 immunotherapy.[8] Combination therapy with αCTLA-4 and αPD-1 antibodies enhances

J Immunother Cancer: first published as 10.1136/jitc-2021-003488 on 19 January 2022. Downloaded from http://jitc.bmj.com/ on April 19, 2024 by guest. Protected by copyright.

efficacy compared with single-agent ICB, likely through complementary mechanisms of systemic $CD4^+$ and $CD8^+$ T cell differentiation and tumor-localized modulation of T effector and regulatory T cells.[9 10] However, tolerability issues with systemically administered αCTLA-4, including with the approved ipilimumab, have restricted clinical use.[11]

Efficacy and tolerability of systemic αCTLA-4 antibody therapy appear to be linked. Increasing ipilimumab dose enhanced both efficacy and side effects.[12] Consistent with the central immune checkpoint function of CTLA-4, side effects may be severe and of systemic autoimmune nature.[13] Interestingly, depletion of intratumoral Treg cells, which overexpress CTLA-4 relative to $CD8^+$ and $CD4^+$ effector T cells, was recently reported to contribute to ipilimumab therapeutic activity. Treg depletion-enhanced αCTLA-4 antibody variants showed improved therapeutic activity in tumor-bearing FcγR-humanized mice.[10] These findings indicate that tumor-localized therapy with Treg-depleting αCTLA-4 antibodies may provide powerful therapeutic activity with reduced side effects compared with currently available αCTLA-4 therapies[14 15] — in particular when combined with validated and safe immunomodulators, for example, blockers of the PD-1/PD-L1 axis or oncolytic viruses (OVs).

Here, we describe and preclinically characterize one such approach. A vaccinia virus (VV)-based oncolytic vector was designed to incorporate both GM-CSF and a novel full-length human recombinant αCTLA-4 antibody selected and characterized for its FcγR-dependent Treg-depleting efficacy (BT-001, $VV_{GM}$-αhCTLA-4). Viruses encoding a matching Treg-depleting mouse surrogate antibody were additionally generated, enabling proof-of-concept studies in syngeneic immune competent mouse tumor models representing inflamed or immune-excluded TMEs sensitive or resistant to ICB.

## MATERIALS AND METHODS

### Cell lines

HEK293T, B16-F10, CT26, A20, EMT6, LL/2, LoVo, MIA PaCa-2, Hs-746 T, SK-OV-3, HCT 116, TF-1, and the NK-92 cell line were purchased from the American Type Culture Collection. Cells stably transfected with human CTLA-4 (293T-CTLA-4) were obtained from Crown Bio. The MC38 cell line was a gift from Mark Cragg.

### Mice

Mice were maintained in local pathogen-free facilities. For all experiments, young adult mice were sex-matched and age-matched and were randomly assigned to experimental groups. C57BL/6 and BALB/c mice were obtained from Taconic, Janvier, or Charles River. Genetically altered strains used were C.129P2(B6)-*Fcer1g*$^{tm1Rav}$ (*Fcer1g*-KO on BALB/c background and BALB/cAnNTac wild type (WT) controls) purchased from Taconic; and B6.129S(C)-*Batf3*$^{tm1Kmm/J16}$ ; *Batf3*-KO on C57BL/6J background and C57BL/6J WT controls) purchased from Jackson Laboratories.

### Human (clinical) samples and ethics

Patient samples were obtained through the Department of Obstetrics and Gynecology and the Department of Oncology at Skånes University Hospital, Lund, Sweden. Ascitic fluid was assessed as single cell suspension that had been isolated. Processing of human tissue is described in online supplemental material.

### Data availability

The assigned accession number for RNAseq data reported in this paper is GEO: GSE176052.

### Statistical analysis

All statistical analyses were carried out using GraphPad Prism V.9.0 (GraphPad Software, La Jolla, California, USA). P values were calculated using Student's t-tests or one-way analysis of variance. The survival periods to the humane end point were plotted using the Kaplan-Meier method with analysis for significance by the log-rank test. Significance was accepted when the p value was $<0.05$.

Supplementary information contains detailed method descriptions for antibody and viral vector generation, and in vitro, ex vivo, and in vivo characterization.

## RESULTS

### Identification and characterization of Treg-depleting αCTLA-4 antibodies

ICB and αCTLA-4 antibody therapy are clinically validated approaches, yet mechanisms underlying αCTLA-4 antibody efficacy are incompletely characterized. Accumulating data suggest that αCTLA-4 antibodies, besides acting to lower the threshold for T cells to recognize tumor antigen and reject tumors, may exert therapeutic activity through depletion of intratumoral Treg cells following antibody interactions with FcγR-expressing effector cells.[17–19] We used the target agnostic F.I.R.S.T discovery platform to screen a large ($>10^{10}$ members) human antibody library (n-CoDeR) for scFv antibodies that bound to target receptors upregulated on Treg, compared with non-Treg CD4 and CD8 effector TILs.[20] Following conversion to full-length IgG format, antibodies were produced, purified, and evaluated for in vivo Treg depletion and antitumor efficacy. The targets of the most functional antibody clones were identified using complementary deconvolution approaches. An array of antibodies and their associated targets capable of depleting Treg cells and improving survival in the T cell-inflamed CT26 mouse tumor model were identified (figure 1A,B). CTLA-4 and αCTLA-4 antibodies were identified among these, and αCTLA-4 mIgG2a mAb depleted intratumoral Treg cells and conferred survival on treatment of animals bearing syngeneic CT26 tumors (figure 1B). Focused screening of human CTLA-4-specific IgG1 antibodies identified several clones with similar in vitro depleting

J Immunother Cancer: first published as 10.1136/jitc-2021-003488 on 19 January 2022. Downloaded from http://jitc.bmj.com/ on April 19, 2024 by guest. Protected by copyright.

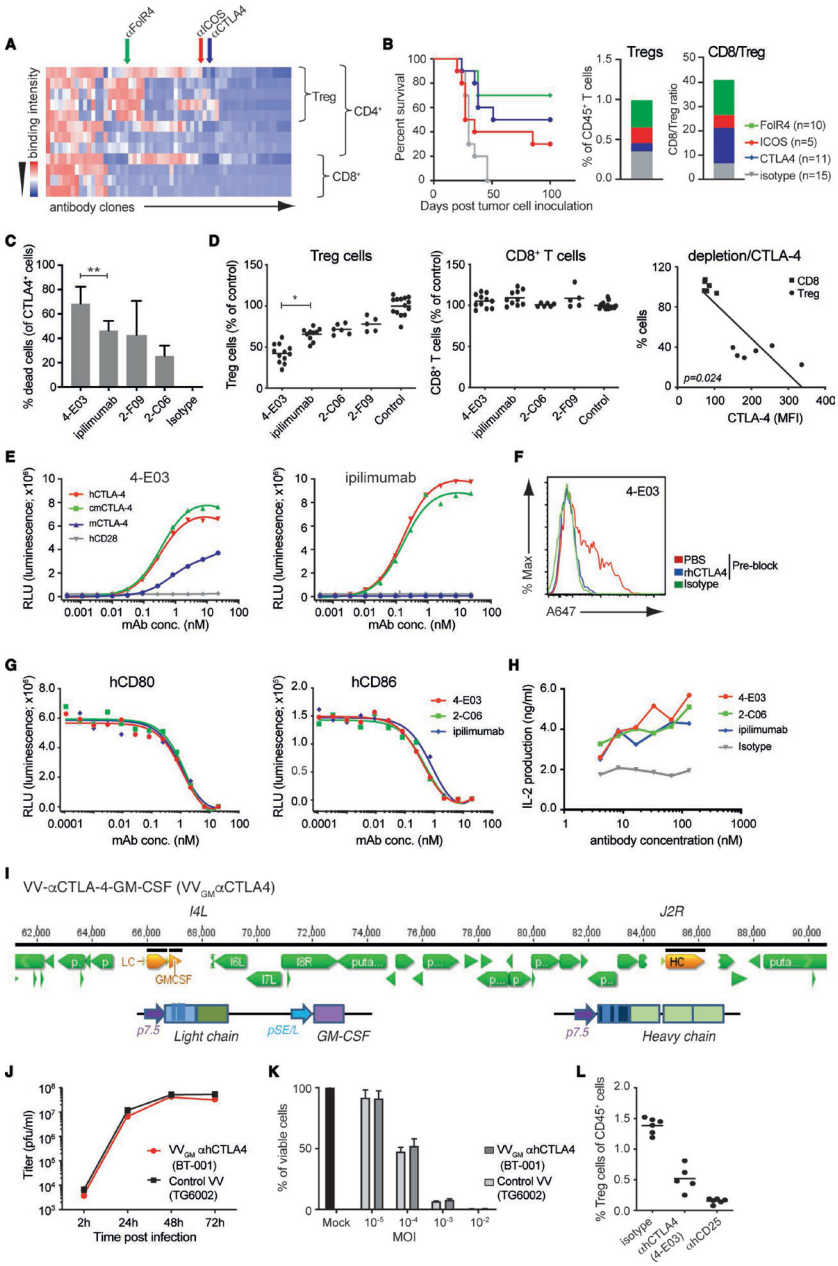


**Figure 1** Generation and characterization of novel Treg-depleting αCTLA-4 mAbs and oncolytic VVs expressing Treg-depleting αCTLA-4 and GM-CSF. (A) Heatmap shows function-first isolated antibody clones (vertical lines) binding to T cells from CT26 tumor-bearing and naïve BALB/c mice. (B) Antibody-mediated survival (left panel) and TIL modulation (right panel) in CT26 tumor-bearing BALB/c mice. Animals with established tumors received four injections (10 mg/kg) of antibodies with indicated Treg-associated specificity or control mIgG2a antibody (n=5–15). (C) CTLA-4-specific mAbs induce ADCC of in vitro-activated $CD4^+$ T cell. Lysed target T cells were identified by FACS. Figure shows mean±SD (n=4–8); **p<0.01 by Student's t-test. (D) Anti-CTLA-4 (IgG1) mAbs mediate Treg depletion in vivo in PBMC-humanized mice. Clone 4-E03 shows enhanced depletion of human Treg cells (left panel) but not $CD8^+$ T cells (right panel) compared with ipilimumab. Each dot represents one mouse. Graph shows mean data from two experiments. *p<0.05 by one-way analysis of variance. Right: Level of 4-E03-induced cell depletion plotted in relation to CTLA-4 expression as determined by flow cytometry. (E) 4-E03 hIgG1 and ipilimumab binding to human, mouse, and cynomolgus CTLA-4 and CD28 by ELISA. (F) 4-E03 IgG1 binding to in vitro-activated CTLA-4-expressing human T cells was preblocked with rhCTLA-4-Fc protein (blue line) (G) 4-E03 and 2-C06 block CD80 and CD86 binding to CTLA-4 by ELISA. (H) Functional ligand blockade in vitro. Graphs show interleukin-2 in supernatants following treatment of in vitro activated human PBMCs with αCTLA-4. A representative donor is shown (n=6). (I) Schematic illustration of the VV vectors used to encode heavy (at J2R locus) and light chains of the αCTLA-4 antibody and GM-CSF (at the I4L locus). (J) Replication kinetics in LoVo cells and (K) oncolytic activity on MIA PaCa-2 cells of $VV_{GM}$-αhCTLA-4 (BT-001). TG6002 (recombinant J2R and I4L deleted VV) was added as control. (L) Functional assessment of αCTLA-4 mAb 4-E03 produced by BT-001-infected MIA PaCa-2 cells in vivo (Treg depletion) as in figure 1D. ADCC, antibody-dependent cell cytotoxicity; FACS, fluorescent-activated cell sorting; ICOS, inducible costimulatory molecule; MOI, multiplicity of infection; PBMC, peripheral blood mononuclear cells; PBS, phosphate-buffered saline; RLU, relative light unit; TIL, tumor-infiltrating lymphocyte; VV, vaccinia virus.



J Immunother Cancer: first published as 10.1136/jitc-2021-003488 on 19 January 2022. Downloaded from http://jitc.bmj.com/ on April 19, 2024 by guest. Protected by copyright.

activity of CTLA-4-expressing human T cells (figure 1C). One clone (4-E03) stood out based on its consistently stronger CTLA-4$^+$ T cell-depleting efficacy compared with other clones when screened across multiple donors (figure 1C). To investigate the in vivo relevance of this clone's apparent stronger depleting activity, we turned to a model where human peripheral blood mononuclear cells (PBMCs) are engrafted into NOD SCID interleukin (IL)-2R gamma$^{-/-}$ (NSG) mice. Owing to a graft-versus host type of interaction human Treg and CD8$^+$ T cells are strongly activated, and show similar co-stimulatory and co-inhibitory molecule expression compared with that observed in human tumors[21] (online supplemental figure 1A). Analyses of NOG-hPBMC CD4$^+$CD25$^+$CD127$^{low}$ Treg and CD8$^+$ T cells indeed revealed similar CTLA-4 expression levels to that observed on T cells obtained from nine patients with ovarian cancer (online supplemental figure 1A). Furthermore, dosing of NOG-hPBMC mice with 10 mg/kg ipilimumab or additional αCTLA-4 antibody clones (2-C06 and 2-F09) demonstrated similar in vivo depleting activity of human CD4$^+$CD25$^+$CD127$^{low}$ Treg cells (figure 1D). However, 4-E03 evoked significantly greater depletion of human Treg cells. Importantly, and consistent with an observed lower expression of CTLA-4 on intratumoral and NOG-hPBMC CD8$^+$ T cells compared with Treg cells (online supplemental figure 1A), and a strong correlation between CTLA-4 expression and antibody-mediated depletion, 4-E03 showed no depletion of human activated CD8$^+$ T cells (figure 1D). Biochemical characterization, in particular HPLC-SEC analyses of 4-E03 antibody preparations, showed >95% monomeric IgG (data not shown), ruling out that 4-E03-enhanced Treg depletion resulted from aggregation of antibody. Consistent with our observation and others' observations, αCTLA-4 mAb Treg depletion was shown to depend on antibody Fc–FcγR interactions. An FcγR binding-impaired variant of 4-E03 ($IgG1_{N297Q}$) showed severely impaired Treg depletion compared with WT FcγR-proficient IgG1 (online supplemental figure 1B).

These findings indicated that 4-E03 binds to a functionally distinct epitope on CTLA-4. We therefore characterized the binding and ligand-blocking activity of 4-E03 relative to ipilimumab and other αCTLA-4 antibodies. All antibodies showed high specificity for the extracellular domain of human CTLA-4 and no observable binding to its closely related human homologue CD28 by ELISA (figure 1E). While 4-E03 and ipilimumab bound with similar potency and efficacy to hCTLA-4 (figure 1E and online supplemental figure 1C), only 4-E03 showed weak but clear cross-reactivity with mouse CTLA-4 (figure 1E). These findings are consistent with the two antibodies binding to distinct epitopes. Further comparative analyses of 4-E03 and ipilimumab assessing binding to endogenously expressed CTLA-4 on in vitro-activated human CD4$^+$ T cells (online supplemental figure 1D and figure 1F), blockade of B7–CTLA-4 interaction (figure 1G), or inhibition of B7–CTLA-4-mediated Tcell suppression (figure 1H), revealed otherwise near identical efficacy and potency. In conclusion, our results indicated that 4-E03 binds to a functionally distinct CTLA-4 epitope, which is associated with stronger Treg depletion but equivalent blockade of B7–CTLA-4 induced T effector cell suppression to the epitope targeted by ipilimumab.

Since 4-E03 cross-reacted only weakly with mouse CTLA-4 (figure 1E), we next focused our screening to identify an appropriate surrogate for in vivo proof-of-concept studies in immunocompetent mouse tumor models. One clone (5-B07), which showed highly specific binding to mouse CTLA-4 transfected CHO cells (online supplemental figure 2A) and mouse CTLA-4 protein (online supplemental figure 2B), blockade of B7–CTLA-4 interactions (online supplemental figure 2C) and similarly strong depletion of intratumoral mouse Treg (online supplemental figure 2D) compared with 4-E03 in the human setting, was identified. Further, αmCTLA-4 (5-B07) conferred antitumor activity and improved survival of CT26 tumor-bearing BALB/c mice (online supplemental figure 2E). As observed with αhCTLA-4 (4-E03) on human cells, αmCTLA-4 (5-B07) depletion of mouse Treg was found to depend on Fc–FcγR interactions. Fc–FcγR binding-proficient but not Fc–FcγR binding-impaired variants of 5-B07 depleted intratumoral Tregs (online supplemental figure 2F).

The similarly pronounced Treg-depleting activity, alongside their similarly high specificity for CTLA-4 and blocking activity of CTLA-4–B7 family interactions, indicated the therapeutic potential of αhCTLA-4 (4-E03) and of αmCTLA-4 (5-B07) as a suitable mode of action (MoA)-matched surrogate.

### Engineering of antibody-encoding OVs for tumor-selective CTLA-4 blockade and Treg depletion

The frequent side effects of αCTLA-4 antibody therapy are consistent with the well-established role of CTLA-4 acting as a central checkpoint to maintain T cell homeostasis and tolerance to self.[13 22] Recent work by Quezada and colleagues, however, has indicated that intratumoral Treg depletion may significantly contribute to ipilimumab clinical activity,[10] and intratumorally delivered Treg-depleting antibodies may afford substantial antitumor activity in mouse tumor models.[15 23] This dual activity of αCTLA-4, acting in central and peripheral compartments, respectively, suggests that localizing αCTLA-4 therapy to tumors may be an attractive strategy to uncouple αCTLA-4 efficacy from toxicity.

We hypothesized that intratumorally delivered OVs engineered to express Treg-depleting αCTLA-4 would represent a particularly attractive means to achieve effective, yet safe, tumor-localized αCTLA-4 therapy. Besides enabling local antibody production and blockade of CTLA-4 receptors and Treg depletion in the TME on infection of tumor cells, OVs are thought to exert both direct and indirect antitumor activity and have been approved for cancer immunotherapy.[24]

We therefore engineered a VV vector, derived from an attenuated Copenhagen strain[25] with clinically proven



J Immunother Cancer: first published as 10.1136/jitc-2021-003488 on 19 January 2022. Downloaded from http://jitc.bmj.com/ on April 19, 2024 by guest. Protected by copyright.

safety and strong immunomodulatory effects observed in global smallpox vaccination programs, and cytolytic and inflammatory cell infiltration-inducing properties in mouse experimental models of immune desert and immune-excluded cancer,[26–29] with full-length αhCTLA-4 or αmCTLA-4 IgG antibody sequences. Variant vectors additionally encoding GM-CSF ($VV_{GM}$-αCTLA-4) (figure 1I), a growth factor inducer and enhancer of myelopoiesis and innate immune cell chemotaxis, were also generated and evaluated for therapeutic efficacy. Following genetic reconstruction, recombinant αCTLA-4 encoding viruses were confirmed to preferentially infect, replicate in (figure 1J), and lyse (figure 1K) tumor cell lines. Tumor cell lines infected with engineered OVs were further shown to produce full-length IgG antibody and GM-CSF transgenes (online supplemental figure 3A,B) with equipotent binding to CTLA-4 receptors (online supplemental figure 2D) and support of GM-CSF-dependent cell proliferation (online supplemental figure 2C) compared with recombinantly produced proteins. 4-E03 produced by BT-001-infected MIA-PaCa-2 tumor cells was also shown to deplete human Treg cells in vivo (figure 1L).

### Intratumoral $VV_{GM}$-αCTLA-4 has antitumor activity associated with tumor-selective CTLA-4 receptor saturation and Treg depletion

$VV_{GM}$-αCTLA-4 antitumor activity was first assessed in the CT26 BALB/c model known to be highly infiltrated by T cells and sensitive to systemic αCTLA-4 antibody treatment.[30] Three intratumoral injections with $7.5\times10^4$, $7.5\times10^5$, or $7.5\times10^6$ plaque-forming units (pfu) of $VV_{GM}$-αCTLA-4 to CT26 tumor-bearing animals demonstrated a dose-dependent antitumor effect, which peaked at $10^6$–$10^7$ pfu, with 6–7/10 animals cured (figure 2A). Treatment with control virus lacking αCTLA-4 antibody and/or GM-CSF transgenes demonstrated a strong dependence on αCTLA-4 antibody (1/10 mice surviving), and a marginal αCTLA-4 enhancing effect of GM-CSF, for therapeutic efficacy (7/10 vs 5/10 mice surviving). Based on the established dose-dependent, αCTLA-4-antibody-dependent, and GM-CSF enhancing effects, we therefore focused our further therapeutic and mechanistic evaluation and characterization on the double transgene-encoding OV ($VV_{GM}$-αCTLA-4) using an intratumorally delivered dose of $1\times10^7$ pfu.

We next assessed tumor and systemic concentrations of αCTLA-4 (figure 2B), GM-CSF (online supplemental figure 4A), and viral particles (online supplemental figure 4B) following intratumoral administration of our transgene-encoding vaccinia OV. Intratumoral injection of $10^7$ $VV_{GM}$-αCTLA-4 infectious particles into syngeneic mouse tumour-bearing immune competent mice generated intratumoral antibody exposure associated with sustained saturation of tumor, but not blood, CTLA-4-expressing cells (figure 2B and online supplemental figure 2A). Similarly, intratumoral administration of $VV_{GM}$-αhCTLA-4 to human tumor xenograft-bearing

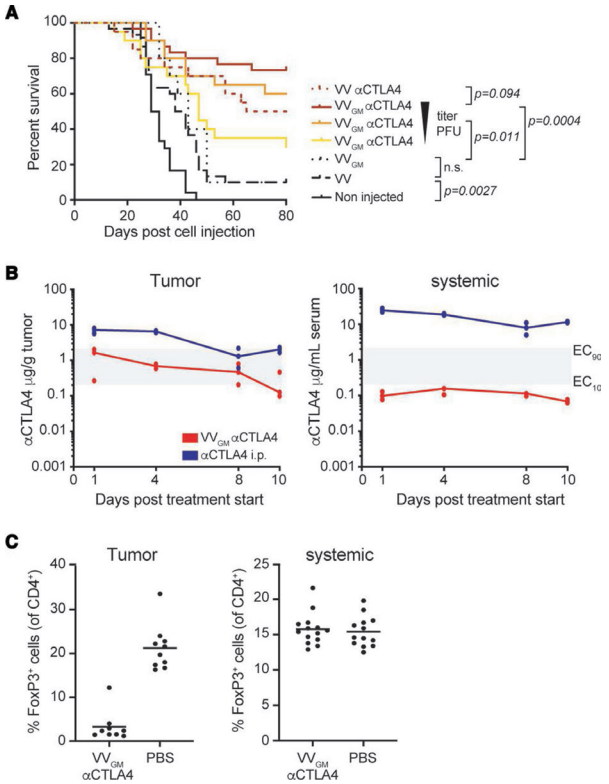


**Figure 2** Intratumoral $VV_{GM}$-αCTLA-4 has in vivo antitumor activity associated with tumor-restricted CTLA-4 receptor saturation and Treg depletion. (A) CT26 tumor-bearing mice were treated with $VV_{GM}$-αCTLA-4 ($7.5\times10^6$, $7.5\times10^5$, or $7.5\times10^4$ pfu), VV-αCTLA-4 ($7.5\times10^6$ pfu), empty VV ($7.5\times10^6$ pfu) (n=20–30 mice/group) or $VV_{GM}$ ($7.5\times10^6$ pfu) (n=10 mice/group). Statistical analysis by log-rank test. (B) Pharmacokinetics of αCTLA-4 in tumors and serum of CT26 tumor-bearing mice after three intratumoral injections (days 0, 2, and 4) of $VV_{GM}$-αCTLA-4 at $10^7$ pfu or after single intraperitoneal injection of 3 mg/kg of αCTLA-4 mAb 5-B07 (n=3 mice/time point). Area in gray indicates $EC_{10}$ to $EC_{90}$ range of CTLA-4 receptor saturation (see online supplemental figure 2A). (C) Numbers of $FoxP3^+$ cells were analyzed by FACS in tumors and spleen at day 10 post $VV_{GM}$-αCTLA-4 injection. Graphs show pooled data from three independent experiments (n=13 mice/group).

immune-deficient mice generated orders of magnitude greater antibody concentrations in tumor compared with blood (online supplemental figure 4C–E). Consistent with intratumoral administration achieving receptor saturating concentrations in tumor but not systemic compartments (figure 2B), intratumoral $VV_{GM}$-αCTLA-4 resulted in near-complete depletion of intratumoral Treg cells but did not affect Treg numbers in spleens of CT26 tumor-bearing BALB/c mice (figure 2C).

Collectively, our results demonstrated that intratumoral administration of αCTLA-4-encoding VV successfully achieved tumor-restricted CTLA-4 receptor saturation and Treg depletion in vivo, supporting its tumor-selective αCTLA-4 therapeutic nature and prompting testing of in vivo efficacy and tolerability in diverse cancer experimental models.

J Immunother Cancer: first published as 10.1136/jitc-2021-003488 on 19 January 2022. Downloaded from http://jitc.bmj.com/ on April 19, 2024 by guest. Protected by copyright.

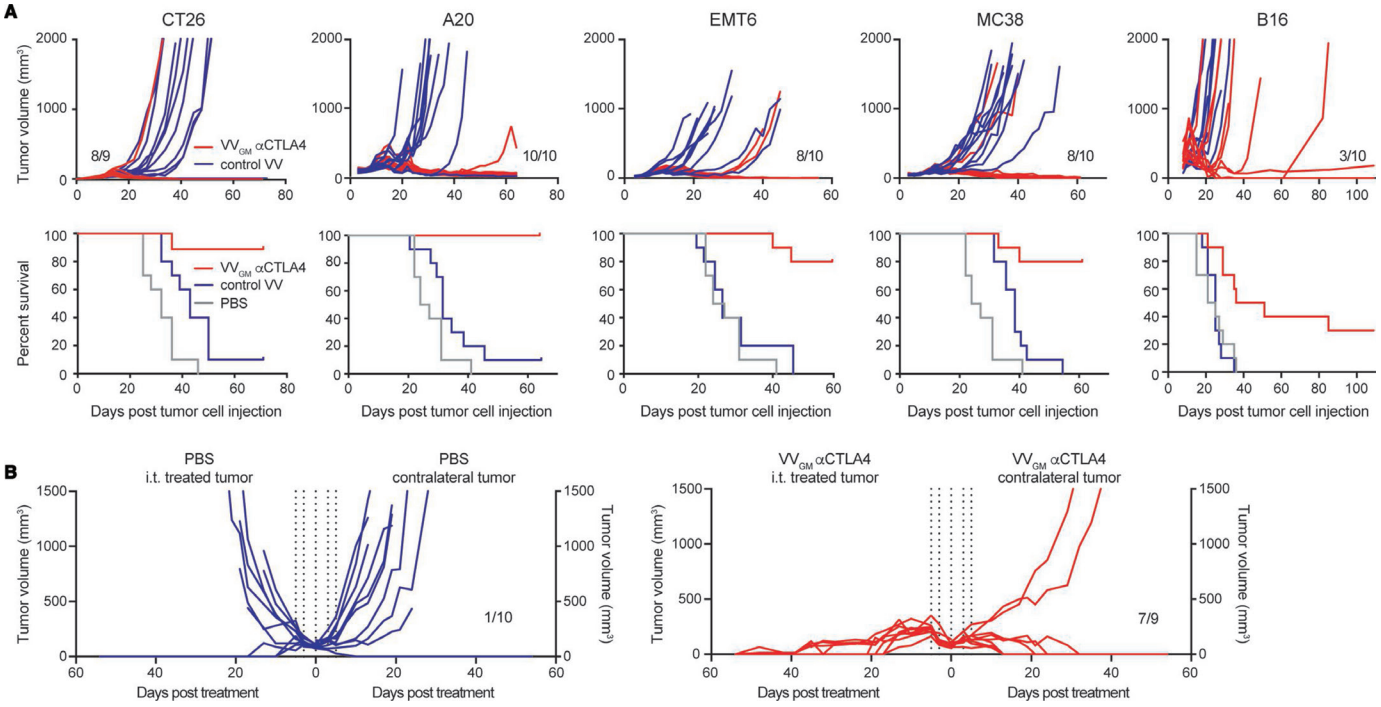


**Figure 3** Intratumoral $VV_{GM}$-αCTLA-4 has broad antitumor activity in syngeneic tumor models spanning inflamed and cold tumor microenvironments. (A) BALB/c mice bearing CT26, A20, or EMT6 tumors, or C57BL/6 mice bearing MC38 or B16 tumors received three intratumoral injections of $VV_{GM}$-αCTLA-4, control virus lacking αmCTLA-4 mAb (VV empty for A20, EMT6, and MC38 or $VV_{GM}$ for CT26 and B16), or PBS. Treatment started when tumors had a volume of ~50 to 100 $mm^3$. Graphs show tumor growth of individual mice and corresponding survival (n=10). (B) CT26 tumor cells were implanted into the right and left flanks of BALB/c mice. Intratumoral injections (vertical dotted lines, same as in A) in right flank tumors with $VV_{GM}$-αCTLA-4 started when tumors reached a volume of ~100 $mm^3$ (n=9–10). VV, vaccinia virus.

## $VV_{GM}$-αCTLA-4 has broad antitumor activity

We proceeded to assess the antitumor activity of intratumoral $VV_{GM}$-αCTLA-4 in a range of immune competent mouse cancer models spanning hematological (A20) and solid cancers of different origin on different genetic mouse backgrounds (CT26 BALB/c colon; EMT6 BALB/c breast, MC38 C57BL/6 colon and B16 C57BL/6 melanoma; figure 3A), representing highly T cell-inflamed (CT26) to immune-excluded (B16) TMEs. The models included those sensitive or resistant to ICB with αCTLA-4 or αPD-1. Strikingly, intratumoral administration of $VV_{GM}$-αCTLA-4 to C57BL/6 or BALB/c mice carrying established syngeneic tumors characterized by diverse immune inflamed types of TME cured the majority (A20=10/10, EMT6=8/10, MC38=8/10 and CT26=8/9 surviving mice) of animals (figure 3A). Equally impressively, in the B16 C57BL/6 model characterized by an immune desert type of TME and resistance to both αPD-1 and αCTLA-4, intratumoral $VV_{GM}$-αCTLA-4 significantly delayed tumor growth and cured 3/10 animals. These results indicated a broad therapeutic potential of $VV_{GM}$-αCTLA-4 in diverse cancer types, including in patients with diverse inflamed and immune-excluded types of TMEs.

## Intratumoral treatment with $VV_{GM}$-αCTLA-4 induces long-lasting systemic antitumor immunity

Preclinical and clinical studies have demonstrated the therapeutic potential of tumor-localized cancer immunotherapy. Intratumoral oncolytic virotherapy, alone[31] or combined with ICB,[8 32] induces durable responses in patients with melanoma cancer. Mechanistically, intratumoral oncovirotherapy has been proposed to induce or enhance inflammatory cell infiltration into injected tumors, resulting in increased tumor antigen presentation, migration to draining lymph nodes, and, following priming, $CD8^+$ T cell trafficking to distant (non-injected) tumor lesions to exert systemic antitumor 'abscopal' effects.[33] In the clinic, such induction of systemic adaptive antitumor memory responses will be critical since patients with cancer may present with widespread disease characterized by metastasized, non-detectable, or uninjectable tumors.

We used a multipronged approach to assess whether intratumoral $VV_{GM}$-αCTLA-4 induced abscopal effects and systemic antitumor immunity. First, using a 'twin tumor model' where tumor cells are subcutaneously grafted to the right and left flanks of each animal but only one tumor is injected with OV and the other is left untreated, abscopal effects can be evaluated and manifested as reduced tumor growth in uninjected tumors. Intratumoral injection of a maximally efficacious $VV_{GM}$-αCTLA-4 dose in CT26 tumor-bearing mice resulted in complete

J Immunother Cancer: first published as 10.1136/jitc-2021-003488 on 19 January 2022. Downloaded from http://jitc.bmj.com/ on April 19, 2024 by guest. Protected by copyright.

(9/9) rejection of injected tumors and near-complete rejection (7/9) of uninjected tumors, indicating a strong abscopal effect (figure 3B). The true abscopal nature of intratumoral OV administration was confirmed twofold. First, non-injected tumors were analyzed and confirmed negative for viral particles (online supplemental figure 5A). Second, intratumoral administration conferred enhanced survival compared with intravenous administration both of therapeutically maximally efficacious ($10^7$ pfu) and suboptimal ($10^5$ pfu) doses of $VV_{GM}$-αCTLA-4 (online supplemental figure 5C). In fact, intratumoral dosing of $10^5$ pfu was at least as efficacious compared with the 100-fold greater intravenous injected dose in rejecting non-injected tumors (online supplemental figure 5B,C). Finally, and consistent with intratumoral OV administration inducing immunological memory characteristic of an adaptive antigen-specific immune response, cured animals were protected against rechallenge with the same (CT26), but not unrelated (Renca), tumors (online supplemental figure 5D).

### $VV_{GM}$-αCTLA-4 elicits robust systemic $CD8^+$ T-cell antitumor immunity

We proceeded to investigate the nature of the systemic antitumor immune response by assessing $VV_{GM}$-αCTLA-4 therapeutic activity in immune intact compared with $CD4^+$ T cell-depleted or $CD8^+$ T cell-depleted CT26 tumor-bearing mice (figure 4A and online supplemental figure 7A). Strikingly, $CD8^+$ T cell depletion completely eliminated $VV_{GM}$-αCTLA-4 antitumor activity. $CD4^+$ T cell depletion reduced, but did not ablate, $VV_{GM}$-αCTLA-4 effects. These data demonstrated that $VV_{GM}$-αCTLA-4 antitumor activity critically depended on $CD8^+$ T cells. We therefore next assessed if intratumoral $VV_{GM}$-αCTLA-4 induced or expanded tumor-specific and virus-specific $CD8^+$ T cells in tumors and in the periphery. CT26 tumor-bearing BALB/c mice were treated intratumorally with $VV_{GM}$-αCTLA-4 or, to mimick clinically available αCTLA-4 regimens, systemically (intraperitoneal) with αmCTLA-4 mAb 5-B07 (3 mg/kg). CT26 tumor-specific and vaccinia-specific $CD8^+$ T cells in tumor and central compartments (spleen) were quantified by two approaches; direct quantification of tumor-specific $CD8^+$ T cells in harvested spleens using CT26 tumor antigen (AH-1)-specific and VV-specific multimers, and by assessment of IFN-$\gamma^+$TNF-$\alpha^+$ $CD8^+$ T cells following ex vivo stimulation of splenocytes (figure 4B) or of TILs with CT26-derived tumor peptide AH-1 and vaccinia-derived peptide S9L8, respectively. Treatment with PBS or VV encoding only GM-CSF were included as controls. As expected, and consistent with intratumoral $VV_{GM}$-αCTLA-4 inducing robust systemic $CD8^+$ T cell-dependent antitumor immunity, intratumoral $VV_{GM}$-αCTLA-4 induced tumor-specific $CD8^+$ T cells both in injected tumors and in peripheral (non-injected tumor and spleen) compartments (figure 4B–D and online supplemental figure 7B) as assessed by ex vivo stimulation of splenocytes or dextramer staining. Impressively, intratumoral $VV_{GM}$-αCTLA-4 expanded tumor-specific $CD8^+$ T cells more effectively compared with systemic αCTLA-4, despite the latter achieving complete saturation of intratumoral CTLA-4 (figure 2B). Control treatment with PBS or virus lacking αCTLA-4 did not induce tumor-specific $CD8^+$ T cells by either read-out. Interestingly, intratumoral treatment with $VV_{GM}$-αCTLA-4 also induced vaccinia-specific $CD8^+$ T cells albeit in low numbers.

Collectively, these data demonstrated that intratumoral $VV_{GM}$-αCTLA-4 induced robust systemic $CD8^+$ T cell-dependent antitumor immunity.

### Intratumorally induced $CD8^+$ T-cell antitumor immunity is FcγR-dependent and cDC1-dependent

The broad antitumor activity, strong expansion of tumor-specific $CD8^+$ T cells in tumor and periphery, and tumor-restricted depletion of Treg cells supported a highly effective and safe treatment with intratumoral $VV_{GM}$-αCTLA-4. To further assess and confirm a role for antibody-mediated Treg depletion underlying antitumor immunity, we compared antitumor effects of intratumoral $VV_{GM}$-αCTLA-4 in CT26 tumor-bearing WT and common gamma chain-deficient (*Fcer1g*$^{-/-}$) BALB/c mice. *Fcer1g*$^{-/-}$ mice lack functional activating Fc gamma receptors and αCTLA-4 antibody in vivo Treg depletion, and associated antitumor activity was previously shown to be activating FcγR-dependent.[10 18] Consistent with αCTLA-4-induced Treg depletion critically underlying intratumoral $VV_{GM}$-αCTLA-4 antitumor immunity, WT (10/10), but not FcγR-deficient animals (3/10), were completely protected and cured from their cancer (figure 5A). The limited but significant antitumor activity observed in FcγR-deficient animals was consistent with our own observation and others' observations that the viral vector (figure 3A) and CTLA-4:B7 blockade *per se* — in the absence of Treg depletion (online supplemental figures 2 and 6) — delayed tumor growth but contributed only limited survival advantage.

Besides affording immune effector-mediated ADCC and antibody-dependent cellular phagocytosis (ADCP) of antibody-coated target cells, FcγRs have been shown to promote tumor antigen cross-presentation,[34] broadening and enhancing the $CD8^+$ T cell antitumor response to encompass normally excluded major histocompatibility complex class II (MHCII)-restricted extracellular tumor antigens. Our findings that intratumoral $VV_{GM}$-αCTLA-4 antitumor immunity was FcγR-dependent and induced more robust expansion of tumor-specific $CD8^+$ T cells compared with systemic αCTLA-4 indicated that it might promote tumor antigen cross-presentation. This notion was reinforced by differential gene expression analyses of tumors harvested from $VV_{GM}$-αCTLA-4-injected compared with viral backbone (VV)-injected and untreated CT26 tumor-bearing mice (figure 5B–D). Besides upregulating *Batf3* and *Irf8 per se*, differential gene expression analyses demonstrated upregulation of type I interferon responses and markers (eg, *CD8a* and *Itgae*), which are associated with cDC1 dendritic cell antigen cross-presentation (figure 5D). FACS analysis data confirmed



J Immunother Cancer: first published as 10.1136/jitc-2021-003488 on 19 January 2022. Downloaded from http://jitc.bmj.com/ on April 19, 2024 by guest. Protected by copyright.

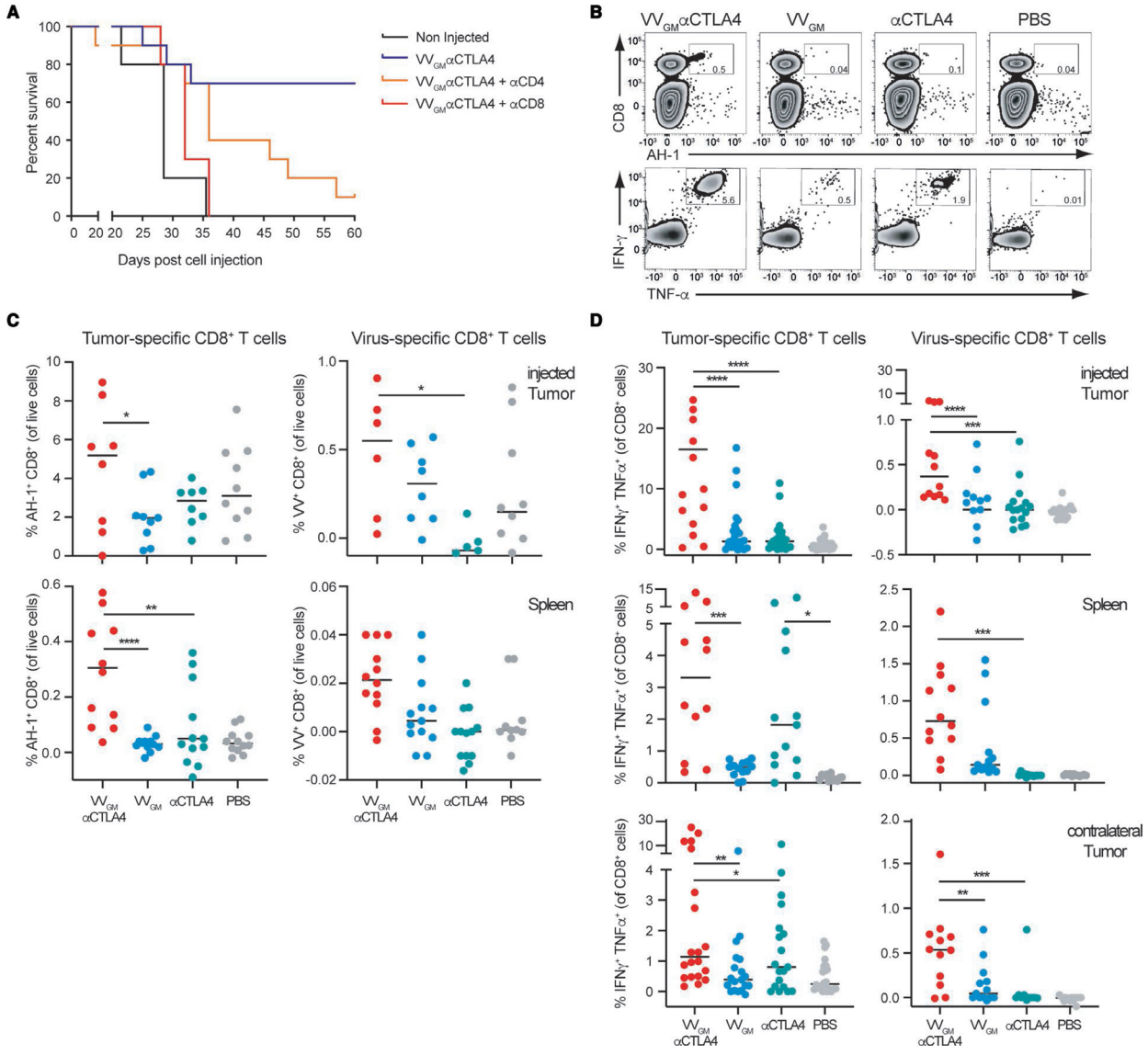


**Figure 4** Intratumoral $VV_{GM}$-αCTLA-4 elicits robust systemic $CD8^+$ T cell-dependent antitumor immunity. (A) BALB/c mice were treated with CD8 or CD4 depleting antibody pre- and post-subcutaneous challenge with CT26 tumor cells. When tumors reached a volume of ~20 to 50 $mm^3$, treatment as in figure 3A commenced. One representative experiment (out of two) is shown with 10 mice per group. (B–D) CT26 tumor-bearing mice were treated intratumorally with VVs or intraperitoneally with αCTLA-4 mAb (clone 5-B07 at 3 mg/kg). Tumor cell suspensions and splenocytes were restimulated ex vivo with VV-specific or CT26 (AH-1)-specific peptide and the percentage of IFN-$\gamma^+$ and TNF$\alpha^+$ $CD8^+$ T cells, or MHC class I-labeled multimer positive $CD8^+$ T cells was quantified by FACS. (B) Flow-cytometry dot plots of AH-1 peptide-positive (upper panel) or cytokine-positive (lower panel) splenocytes. Quantification of (C) antigen-specific and (D) IFN-$\gamma^+$/TNF$\alpha^+$ $CD8^+$ T cells in indicated organs. Each dot represents one mouse (n=3–6 experiments). *p<0.05, **p<0.01, ***p<0.001, ****p<0.0001 by one-way analysis of variance. IFN-γ, interferon gamma; VV, vaccinia virus.

a significant increase in $CD103^+Sirp\alpha^-$ cDC1s in tumors of $VV_{GM}$-αCTLA-4-treated mice compared with control groups (figure 5E). Additional signatures supported the aforementioned characterized $CD8^+$ T cell-dependent (and potentially NK-cell-mediated granzyme-dependent) tumor cytolysis underlying triggering and actuation of $VV_{GM}$-αCTLA-4 antitumor immunity (figure 5B,C).

To assess a role for antigen cross-presentation in $VV_{GM}$-αCTLA-4-induced antitumor immunity, we used mice lacking the transcription factor *Batf3* (*Batf3*$^{-/-}$ mice). *Batf3*$^{-/-}$ mice lack $CD8\alpha^+$ cDC1 dendritic cells and as a consequence show defective antigen cross-presentation and severely impaired $CD8^+$ T cell responses to viruses during infection and to tumor antigens in mouse experimental models of cancer.[16] Further, cDC1s and antigen cross-presentation are known to mediate therapeutic activity of immune checkpoint blockers including αCTLA-4.[35] We therefore compared antitumor activity of intratumoral $VV_{GM}$-αCTLA-4 in *Batf3*$^{+/+}$ and *Batf3*$^{-/-}$ C57BL/6 mice transplanted with MC38 tumors. Strikingly, *Batf3*-deficiency abrogated intratumoral $VV_{GM}$-αCTLA-4 antitumor immunity as demonstrated by 0/8 *Batf3*$^{-/-}$ compared with 9/9 WT mice surviving (figure 5F). Collectively, these results demonstrated that $VV_{GM}$-αCTLA-4



J Immunother Cancer: first published as 10.1136/jitc-2021-003488 on 19 January 2022. Downloaded from http://jitc.bmj.com/ on April 19, 2024 by guest. Protected by copyright.

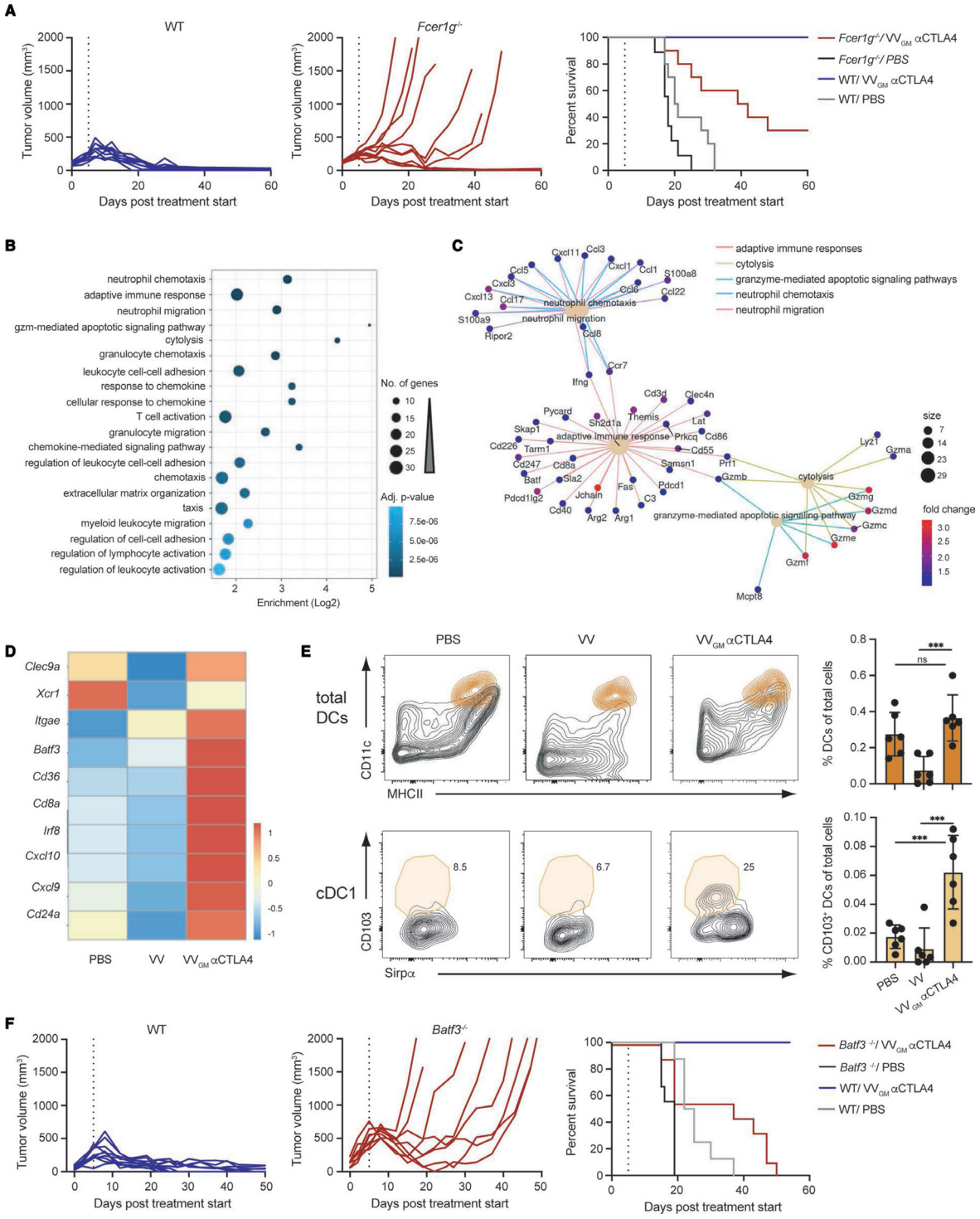


**Figure 5** Intratumorally induced CD8$^+$ T cell antitumor immunity is FcγR-dependent and cDC1-dependent. (A) CT26 tumor-bearing WT and *Fcer1g*$^{-/-}$ BALB/c mice received intratumoral injections of $VV_{GM}$-αCTLA-4 or PBS as in figure 3A. Graphs show tumor volume (left and center panels) and mouse survival (right panel). Vertical lines indicate the end of the treatment. (n=10 mice/group) (B) GO terms enriched in the set of 352 differentially expressed genes, either upregulated or downregulated, in CT26 tumors treated with $VV_{GM}$-αCTLA-4 versus VV empty. The 20 enriched terms with the lowest adjusted p value are shown. (C) Network view of the differentially expressed genes associated with the five most enriched GO terms from (B). Only genes upregulated were found associated with these five enriched GO terms. (D) Heatmap representation of cDC1-associated transcripts differentially expressed after treatment with $VV_{GM}$-αCTLA-4 or VV empty. (E) Representative FACS plots and summarized quantitation of total DCs and cDC1s in tumors following treatment. DCs were gated as described in supplemental information and further defined as CD103$^+$/Sirpα$^-$ cDC1s. ***p<0.001 by one-way analysis of variance. (F) MC38 tumor-bearing WT and *Batf3*$^{-/-}$ C57BL/6 mice received intratumoral injections of $VV_{GM}$-αCTLA-4 or PBS as in figures 3A and 5A. Graphs show tumor volume (left and center panels) and mouse survival (right panel). Vertical lines indicate the end of the treatment. (n=8–10 mice/group).DC, dendritic cell; ns, not significant; VV, vaccinia virus; WT, wild type.



J Immunother Cancer: first published as 10.1136/jitc-2021-003488 on 19 January 2022. Downloaded from http://jitc.bmj.com/ on April 19, 2024 by guest. Protected by copyright.

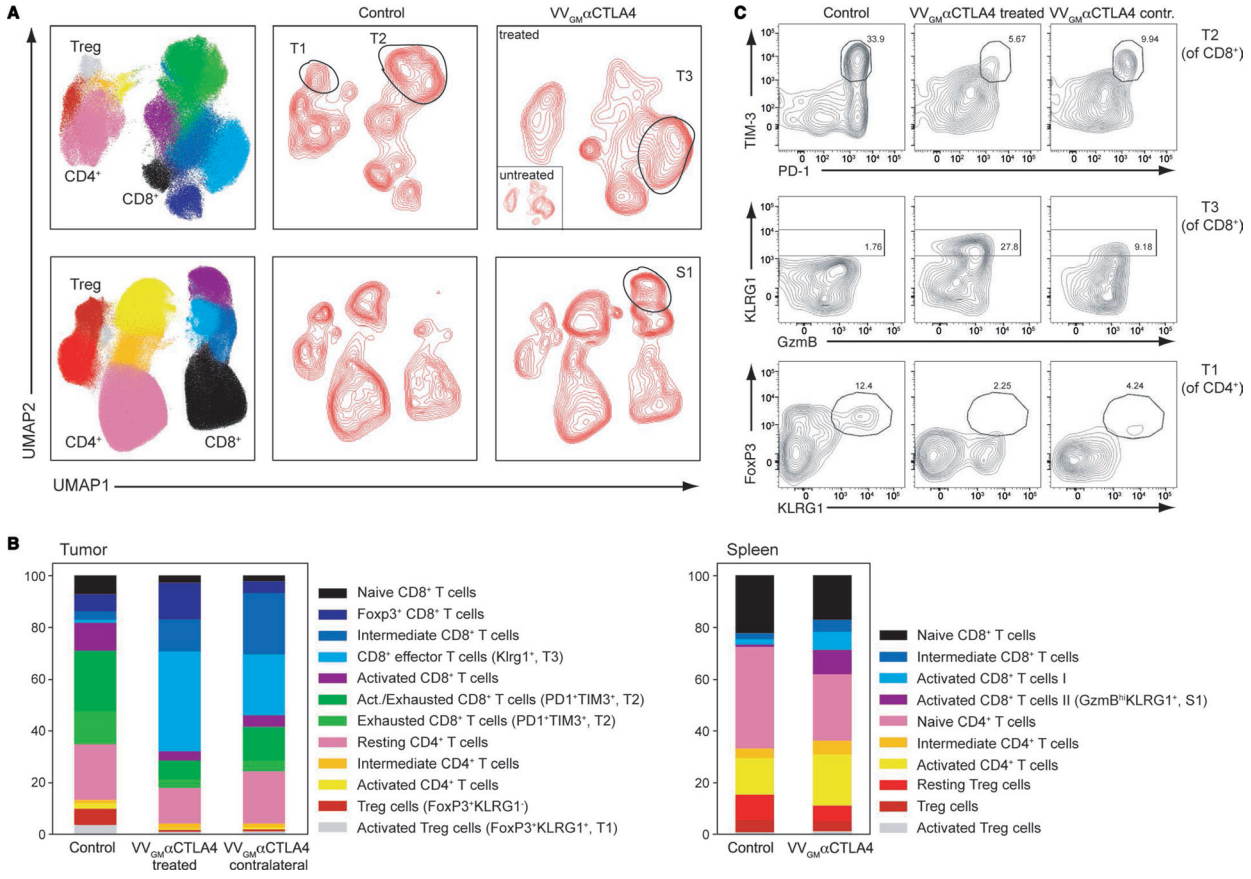


**Figure 6** Intratumoral $VV_{GM}$-αCTLA-4 expands peripheral effector $CD8^+$ T cells and reduces Treg and exhausted $CD8^+$ T cells. CT26 'twin' tumor-bearing BALB/c mice were treated intratumorally (right flank tumors only) with $VV_{GM}$-αCTLA-4 or PBS. Spleens and injected and contralateral tumors were collected on day 10 post-treatment and stained with a high-dimensional panel designed to identify T-cell populations. (A) Intratumoral $VV_{GM}$-αCTLA-4 reduced activated $CD4^+$ Treg cells ($FoxP3^+KLRG1^+$, 'T1'), reduced exhausted $CD8^+$ T cells ($PD1^+TIM3^+$, and 'T2'), and expanded activated effector $CD8^+$ T cells ($KLRG1^+$ and 'T3') in injected and uninjected tumors (upper panel) and expanded activated $CD8^+$ T cells in spleen (S1, lower panel) (B) shows quantification of data illustrated in A. One representative experiment (out of three) with five mice/group is shown. (C) Flow cytometry plots show characteristic markers of selected intratumoral T-cell clusters. VV, vaccinia virus.

has both FcγR-dependent and cDC1-dependent antitumor activity, identifying intratumorally induced Treg-depletion and tumor antigen cross-presentation as major mechanisms, and intratumoral CTLA-4–B7-blockade and oncolysis as supporting mechanisms, underlying intratumoral $VV_{GM}$-αCTLA-4 induced $CD8^+$ T cell antitumor immunity.

### Intratumoral $VV_{GM}$-αCTLA-4 expands peripheral effector $CD8^+$ T cells and reduces Treg and exhausted $CD8^+$ T cells

We proceeded to qualitatively characterize how intratumoral $VV_{GM}$-αCTLA-4 modulates TIL responses in injected and flanking tumors, and in the periphery. Using multicolor flow-cytometry and a high-dimensional antibody panel designed to identify functionally distinct antitumor and protumor TIL subsets, 12 T cell clusters across treatment groups were identified (figure 6 and online supplemental figure 7C). Strikingly, intratumoral $VV_{GM}$-αCTLA-4 eliminated exhausted ($PD\text{-}1^+TIM\text{-}3^+$) $CD8^+$ T cells and robustly expanded non-exhausted $KLRG1^+$ effector $CD8^+$ T cells in injected tumors compared with mock-treated animals (figure 6). At the same time, and consistent with our previously mentioned findings, intratumoral $VV_{GM}$-αCTLA-4 effectively depleted $CTLA\text{-}4^+$ intratumoral Tregs, including $KLRG1^+$ Tregs, which are known to express high levels of CTLA-4 and to be particularly suppressive (figure 6).[36]

Assessment of flanking distal tumors, which had not been injected with antibody-encoding virus, revealed similar but less profound modulation of TIL by intratumoral $VV_{GM}$-αCTLA-4. Further, and in keeping with our observations that intratumoral administration of the αCTLA-4-encoding OV expanded tumor-specific $CD8^+$ T cells in the periphery (figure 4B–D), intratumoral $VV_{GM}$-αCTLA-4 induced activated granzyme $B^+$ ($KLRG1^+$) $CD8^+$ T cell subsets in spleen (figure 6A,C). Finally, and consistent with the antibody-encoding virus achieving tumor-restricted Treg depletion, Treg populations that were depleted in tumor beds were largely unaltered in spleen by intratumoral $VV_{GM}$-αCTLA-4 (figure 6A).

J Immunother Cancer: first published as 10.1136/jitc-2021-003488 on 19 January 2022. Downloaded from http://jitc.bmj.com/ on April 19, 2024 by guest. Protected by copyright.

### Intratumoral $VV_{GM}$-αCTLA-4 combines with αPD-1 to reject 'cold' distal tumors

Our observations demonstrated that $VV_{GM}$-αCTLA-4 acted locally in injected tumors, principally by mechanisms involving αCTLA-4 mAb-dependent tumor antigen cross-presentation and Treg-depletion, to 'ignite' systemic adaptive antitumor immunity and robust peripheral tumor-specific $CD8^+$ T cell expansion. These findings indicated that $VV_{GM}$-αCTLA-4 might synergize with therapeutic agents that help mobilize $CD8^+$ T cells to the tumor. αPD-1 is thought to act principally by reversal of T cell exhaustion[37 38] and possibly by mobilizing stem-like memory $CD8^+$ T cells to tumors.[39 40] Despite αPD-1's documented ability to improve survival in multiple solid cancers of different origin, it does not improve outcome in patients with poorly immune infiltrated 'cold tumors',[41] which perhaps represent the greatest unmet medical need in cancer therapy today. Based on their apparently different and potentially complementary mechanism of action, we therefore next examined synergizing effects of αPD-1 and $VV_{GM}$-αCTLA-4 with a focus on ICB-resistant, poorly immune infiltrated and poorly immunogenic cold cancers using B16 C57BL/6 as a model system. Our previous data had demonstrated that B16 tumors responded poorly to ICB therapy, including to clinically relevant systemic administration of αPD-1 (10 mg/kg), αCTLA-4 (10 mg/kg) or the combination thereof (online supplemental figure 8A). So as to mimick the clinical situation where palpable large tumors will be injected with the antibody-encoding virus, but small or undetectable metastasized lesions cannot be injected, we established a twin-tumor B16/C57BL6 model where the animals carry one 'large' and one 'small' tumor, and where only the large tumor was injected intratumorally with $VV_{GM}$-αCTLA-4. Resistance to αPD-1 was confirmed by lack of tumor growth inhibition or survival benefit following systemic treatment with a maximally efficacious dose of 10 mg/kg (figure 7A). As previously observed, single-agent treatment with $VV_{GM}$-αCTLA-4 significantly reduced tumor growth of the primary injected tumor (figures 3 and 7B). However, intratumoral $VV_{GM}$-αCTLA-4 only induced a slight delay of uninjected tumor's growth

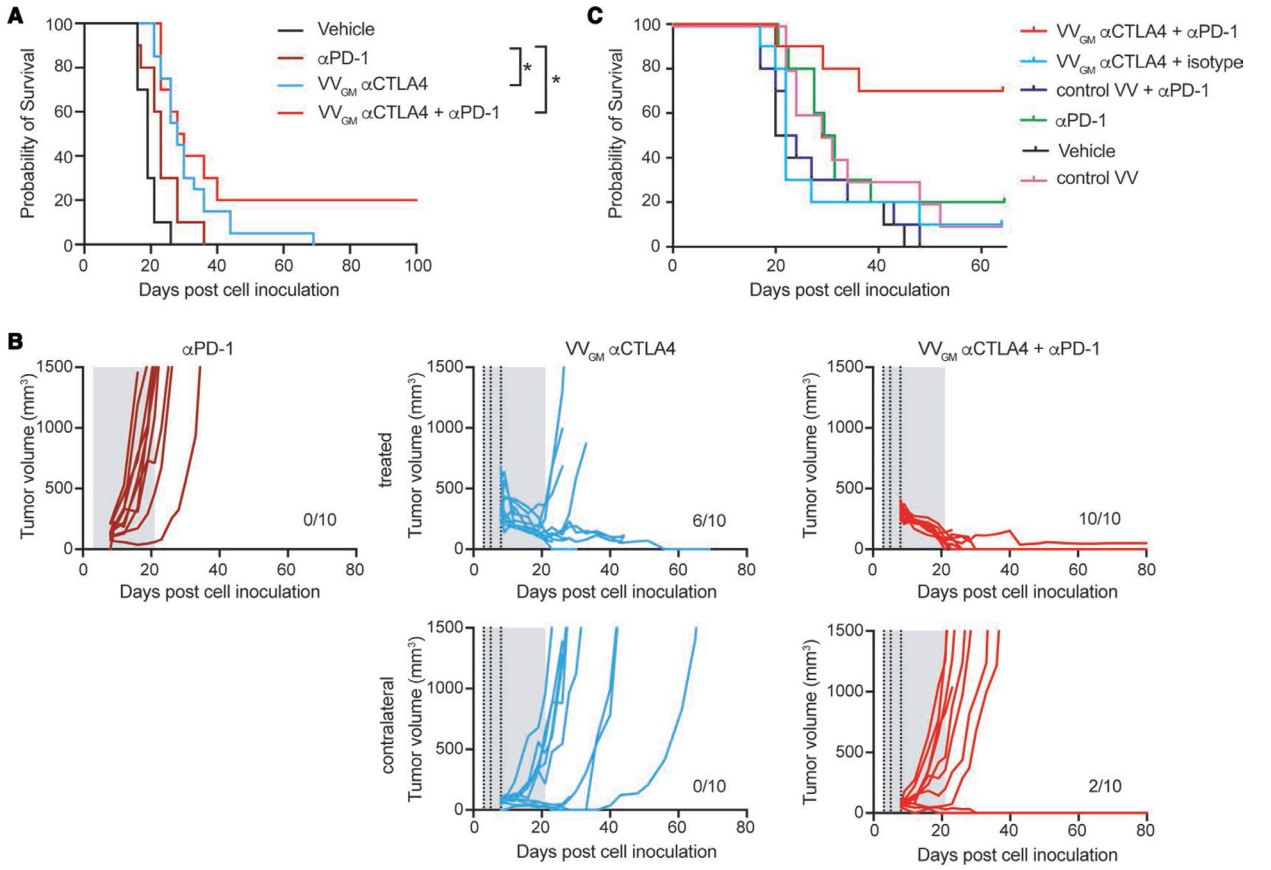


**Figure 7** Intratumoral $VV_{GM}$-αCTLA-4 synergizes with αPD-1 to reject 'cold' immune checkpoint blockade-resistant tumors. (A,B) C57BL/6 mice carrying two B16 tumors, one large ($5\times10^5$ cells, treated tumor) and one small tumor ($1\times10^5$ cells, contralateral side) received three intratumoral injections with $VV_{GM}$-αCTLA-4 (vertical dotted lines) and/or intraperitoneal αPD-1 (29F.1A12, 10 mg/kg; two times per week for 3 weeks, gray area). (A) Survival (n=10–20), *p<0.05 by log-rank test. (B) Tumor growth curves of intratumorally injected and contralateral tumors. (C) A20 tumor-bearing BALB/c mice were treated thrice with $VV_{GM}$-αCTLA-4 intratumorally (at a suboptimal dose of $1\times10^5$ pfu), αPD-1 intraperitoneally (RMP1-14, full dose of 10 mg/kg) or the combination of both when tumors had reached a volume of ~135 $mm^3$. Graph shows animal survival (n=10). VV, vaccinia virus.



J Immunother Cancer: first published as 10.1136/jitc-2021-003488 on 19 January 2022. Downloaded from http://jitc.bmj.com/ on April 19, 2024 by guest. Protected by copyright.

(figure 7B), which did not translate into animal survival (figure 7A). In contrast, combined treatment with intratumoral $VV_{GM}$-αCTLA-4 and systemic αPD-1 significantly inhibited injected and uninjected tumor growth, resulting in ~20% of animals bearing cured in this ICB treatment-resistant model of cold cancer (figure 7A). Further consistent with $VV_{GM}$-αCTLA-4 being able to convert cold, ICB-resistant tumors toward an inflamed, ICB responsive, phenotype, combined treatment with $VV_{GM}$-αCTLA-4 (but not αPD-1 alone) induced a strong influx of T cells into B16 tumors, which became similarly densely T cell rich compared with inflamed CT26 tumors (online supplemental figure 8B). Finally, and consistent with a broad potential to treat cold tumors, $VV_{GM}$-αCTLA-4 significantly improved survival also of Lewis Lung tumor-bearing mice (online supplemental figure 8D). Like B16, this model was poorly T cell infiltrated and did not respond to clinically relevant, systemic, dual checkpoint αCTLA-4/αPD1 blockade (online supplemental figure 8C).

The indicated synergizing effects of combined intratumoral $VV_{GM}$-αCTLA-4 and systemic αPD-1 were confirmed in BALB/c mice transplanted with syngeneic A20 tumors. This model was shown to be semiresponsive to αPD-1 with ~20% of animals being cured by full therapeutic intraperitoneal dosing (10 mg/kg) (figure 7C). While optimal therapeutic dosing with intratumoral $VV_{GM}$-αCTLA-4 was fully protective (10/10 animals cured, figure 3), suboptimal treatment with 1/100 of the optimal dose showed insignificant tumor growth inhibition and no survival advantage. When therapeutic intraperitoneal αPD-1 and subtherapeutic intratumoral $VV_{GM}$-αCTLA-4 were combined, the majority of animals (7/10) were cured (figure 7C).

## DISCUSSION

We here provide in vivo proof of concept that intratumoral administration of oncovirally encoded Treg-depleting αCTLA-4 has stronger and broader antitumor activity compared with approved systemic αCTLA-4 regimens yet, through its tumor-restricted nature of exposure, is indicated to be safe and well tolerated. Intratumoral $VV_{GM}$-αCTLA-4 induced stronger expansion of tumor-specific $CD8^+$ T cells compared with systemic recombinant αCTLA-4 and had antitumor activity in poorly immune infiltrated cold syngeneic mouse tumor models resistant to clinically relevant dosing with systemic αCTLA-4 and αPD-1. Remarkably, our observations suggest that the potent systemic antitumor immunity induced by oncoviral αCTLA-4 derived strictly from 'immune-igniting' effects in injected tumors; intratumoral $VV_{GM}$-αCTLA-4 was not associated with virus spread or antibody exposure to distal uninjected tumors, but rather achieved tumor-restricted CTLA-4 receptor saturation and Treg depletion. These observations have important implications both for expected clinical efficacy and tolerability of intratumoral $VV_{GM}$-αCTLA-4. From an efficacy perspective, they demonstrate that local administration of oncovirally encoded αCTLA-4 may provide greater therapeutic benefit compared with available (ipilimumab) and Treg-depletion-optimized[10] or 'masked',[42] systemic αCTLA-4 antibody regimens, as well as compared with previously described OV approaches encoding non-Treg depletion-optimized αCTLA-4.[43] At a mechanistic level, $VV_{GM}$-αCTLA-4-induced FcγR-dependent Treg depletion and cDC1 antigen cross-presentation are likely to underly both the observed robust $CD8^+$ T cell expansion and synergism with αPD-1 to reject cold tumors. Besides mediating induction of endogenous antitumor immune responses[16] and efficacy of systemic checkpoint blockade therapy,[35 44 45] cDC1s promote the proliferative response of intratumoral $CD8^+$ TILs, expand the pool of $TCF1^+$ stem-like precursors, and induce generation of $TIM\text{-}3^+$ terminal effectors during αPD-1 therapy.[46] Similarly, Treg depletion achieved with mAb to costimulatory or coinhibitory receptors, for example, IL-2R and CTLA-4, may promote $CD8^+$ effector function and synergize with αPD-1.[47 48] With regard to development of 'dual activity' immune modulatory antibodies that reduce Treg and expand antitumor $CD8^+$ T cells, accumulating data demonstrate the importance of both target biology, fine-tuning of effector $CD8^+$ T cell-enhancing and Treg-depleting properties, as well as delivery regimen. For example, it was recently demonstrated that FcγR-competent non-ligand blocking antibodies to IL-2R, which deplete Treg but do not starve $CD8^+$ effector T cells of critical (IL-2-mediated) growth survival signaling, have superior therapeutic potential in cancer therapy compared with ligand-blocking αIL-2R antibodies.[47] Analogously, but differently, we recently reported that antibodies to 4-1BB can be made to deplete Tregs or promote effector T cell expansion by antibody isotype switching (altering FcγR-engagement), but that harnessing both mechanisms required sequential administration or hinge-engineering.[21] As described herein, spatial restriction of Treg-depleting, checkpoint blocking, αCTLA-4 to injected tumors appears to be a particularly promising approach for harnessing maximal therapeutic activity of immune modulatory αCTLA-4 antibodies, when used alone or in combination with synergizing checkpoint blockade therapy for example, αPD-1/L1.

Several observations support optimizing Treg depletion in αCTLA-4 for tumor-localized therapy. First, independent studies have established that therapeutic efficacy of αCTLA-4 depends on and correlates with Treg depletion.[10 18] Herein presented data on therapeutic activity of Treg-depleting recombinant and oncovirally encoded αCTLA-4 antibodies, which showed strong curative effect in FcγR-proficient (Treg-depleting) antibody Fc formats and hosts compared with their FcγR-deficient (non-depleting) counterparts, support this notion. Second, while clinical outcome of patients with melanoma treated with ipilimumab was recently reported to correlate with FcγR-engagement and Treg-depletion, data from our T cell humanized mouse model suggests ipilimumab has limited depleting activity compared with the herein vectorized αCTLA-4 antibody 4-E03 against human Treg cells expressing intratumorally relevant levels of CTLA-4.



J Immunother Cancer: first published as 10.1136/jitc-2021-003488 on 19 January 2022. Downloaded from http://jitc.bmj.com/ on April 19, 2024 by guest. Protected by copyright.

Further, whereas clinically tolerated doses of ipilimumab (1–3 mg/kg, depending on indication and regimen) are associated only with subsaturating CTLA-4 receptor occupancy and submaximal effect,[12 49] our data demonstrate that oncolytic vectorization and intratumoral administration can generate therapeutically optimal exposure in an apparently safe manner, even with Treg depletion-enhanced αCTLA-4. Finally, and supporting our vectorization of a Treg depletion-enhanced and checkpoint blocking 'dual activity' αCTLA-4 antibody, antibody-mediated CTLA-4 blockade was recently shown to synergize with FcγR-dependent depletion in improving tumor-specific $CD8^+$ T cell responses. Antibody blockade of CTLA-4 functionally destabilized intratumoral Treg and promoted B7–CD28 costimulation and antitumor $CD8^+$ T effector function through processes involving altered glycolysis and competition for B7 ligands.[50]

The fact that full therapeutic dosing achieved tumor-restricted αCTLA-4 exposure indicates that severe toxicities associated with sustained systemic Treg depletion, for example, those observed in the FoxP3-DTR mouse model,[51] are unlikely to manifest. Similarly, since αCTLA-4 checkpoint blockade effects will be restricted to TILs with tumor-antigen specificity, untoward self-reactivity associated with systemic αCTLA-4 should be minimal. In contrast, but consistent with the well-documented central immune checkpoint nature of CTLA-4,[52 53] αCTLA-4 side effects associated with systemic administration, that is, body-wide antibody exposure, may be of severe autoimmune nature and can have fatal consequences.[13 22]

Taken together, therefore, while efficacy and tolerability of available αCTLA-4 regimens are considered to be linked and dose-dependent precluding use of full therapeutic dosing, our findings strongly suggest that spatial restriction of vectorized Treg-depleting αCTLA-4 is able to overcome these current limitations, uncoupling efficacy from tolerability. A clinical study investigating intratumoral $VV_{GM}$-αhCTLA-4 (BT-001) alone and in combination with αPD-1 in metastatic or advanced solid tumors is open and enrolling patients (NCT04725331).

**Author affiliations**
[1]Department of Research, BioInvent International AB, Lund, Sweden
[2]Department of Research, Transgene SA, Illkirch-Graffenstaden, France
[3]Antibody and Vaccine Group, Centre for Cancer Immunology, Cancer Sciences Unit, Faculty of Medicine, University of Southampton, Southampton, UK

**Acknowledgements** We thank Drs Mark Cragg and Stephen Beers (University of Southampton) for their valuable advice and critical review of the manuscript. We thank Huguette Schultz, Chantal Hoffmann, Eline Winter, Fadi Azar, Julie Hortelano, Dominique Villeval, Murielle Gantzer, Virginie Nourtier, Juliette Kempf, Mathilda Kovacek, and Ann-Helen Fischer for their technical contributions.

**Contributors** MS, J-BM, EQ, and BF conceived the project and wrote the manuscript. MS, J-BM, LF, MR, CR, PH, NS, LM, JF, CS, PK, JD, MB and KLC designed, performed, and analyzed the experiments. FJ contributed to the data analysis. IT contributed scientifically. BF accepts full responsibility for the work and/or the conduct of the study, had access to the data, and controlled the decision to publish.

**Funding** All support for this article was entirely provided by BioInvent International AB and Transgene SA.

**Competing interests** MS, MR, PH, LM, CS, FJ, MB, IT, and BF are employees, MS, MR, LM, FJ, MB, IT, and BF are shareholders of BioInvent International. KLC received funding from BioInvent. J-BM, LF, CR, NS, PK, JD, JF, and EQ are employees and shareholders of Transgene.

**Patient consent for publication** Not applicable.

**Ethics approval** This study does not involve human subjects. All procedures were approved by the local ethical committee for experimental animals (Malmö/Lunds Djurförsöksetiska Nämnd, at BioInvent under permit numbers 17196/2018 or 2934/2020, or at Transgene APAFIS Nr21622 project 2019072414343465) and performed in accordance with local ethical guidelines. Ethical approval was obtained by the ethics committee of Skåne University Hospital. Informed consent was provided in accordance with the Declaration of Helsinki.

**Provenance and peer review** Not commissioned; externally peer reviewed.

**Data availability statement** The datasets generated during and/or analyzed during this current study have been deposited or are available from the corresponding author on reasonable request. The assigned accession number for RNAseq data reported in this paper is GEO: GSE176052.

**Supplemental material** This content has been supplied by the author(s). It has not been vetted by BMJ Publishing Group Limited (BMJ) and may not have been peer-reviewed. Any opinions or recommendations discussed are solely those of the author(s) and are not endorsed by BMJ. BMJ disclaims all liability and responsibility arising from any reliance placed on the content. Where the content includes any translated material, BMJ does not warrant the accuracy and reliability of the translations (including but not limited to local regulations, clinical guidelines, terminology, drug names and drug dosages), and is not responsible for any error and/or omissions arising from translation and adaptation or otherwise.

**Open access** This is an open access article distributed in accordance with the Creative Commons Attribution Non Commercial (CC BY-NC 4.0) license, which permits others to distribute, remix, adapt, build upon this work non-commercially, and license their derivative works on different terms, provided the original work is properly cited, appropriate credit is given, any changes made indicated, and the use is non-commercial. See http://creativecommons.org/licenses/by-nc/4.0/.

**ORCID iD**
Björn Frendéus http://orcid.org/0000-0003-3177-8686

## REFERENCES

1 Hodi FS, O'Day SJ, McDermott DF, *et al*. Improved survival with ipilimumab in patients with metastatic melanoma. *N Engl J Med* 2010;363:711–23.
2 Larkin J, Chiarion-Sileni V, Gonzalez R, *et al*. Combined nivolumab and ipilimumab or monotherapy in untreated melanoma. *N Engl J Med* 2015;373:23–34.
3 Topalian SL, Hodi FS, Brahmer JR, *et al*. Safety, activity, and immune correlates of anti-PD-1 antibody in cancer. *N Engl J Med* 2012;366:2443–54.
4 Sharma P, Hu-Lieskovan S, Wargo JA, *et al*. Primary, adaptive, and acquired resistance to cancer immunotherapy. *Cell* 2017;168:707–23.
5 Chen DS, Mellman I. Oncology meets immunology: the cancer-immunity cycle. *Immunity* 2013;39:1–10.
6 Gajewski TF, Schreiber H, Fu Y-X. Innate and adaptive immune cells in the tumor microenvironment. *Nat Immunol* 2013;14:1014–22.
7 Wagner J, Wickman E, DeRenzo C, *et al*. CAR T cell therapy for solid tumors: bright future or dark reality? *Mol Ther* 2020;28:2320–39.
8 Ribas A, Dummer R, Puzanov I, *et al*. Oncolytic virotherapy promotes intratumoral T cell infiltration and improves anti-PD-1 immunotherapy. *Cell* 2017;170:1109–19.
9 Wei SC, Sharma R, Anang N-AAS, *et al*. Negative co-stimulation constrains T cell differentiation by imposing boundaries on possible cell states. *Immunity* 2019;50:1084–98.
10 Arce Vargas F, Furness AJS, Litchfield K, *et al*. Fc effector function contributes to the activity of human anti-CTLA-4 antibodies. *Cancer Cell* 2018;33:649–63.
11 Postow MA, Chesney J, Pavlick AC, *et al*. Nivolumab and ipilimumab versus ipilimumab in untreated melanoma. *N Engl J Med* 2015;372:2006–17.
12 Bertrand A, Kostine M, Barnetche T, *et al*. Immune related adverse events associated with anti-CTLA-4 antibodies: systematic review and meta-analysis. *BMC Med* 2015;13:211.
13 Tivol EA, Borriello F, Schweitzer AN, *et al*. Loss of CTLA-4 leads to massive lymphoproliferation and fatal multiorgan tissue destruction,

J Immunother Cancer: first published as 10.1136/jitc-2021-003488 on 19 January 2022. Downloaded from http://jitc.bmj.com/ on April 19, 2024 by guest. Protected by copyright.

revealing a critical negative regulatory role of CTLA-4. *Immunity* 1995;3:541–7.
14 Marabelle A, Kohrt H, Levy R. Intratumoral anti-CTLA-4 therapy: enhancing efficacy while avoiding toxicity. *Clin Cancer Res* 2013;19:5261–3.
15 Marabelle A, Kohrt H, Sagiv-Barfi I, *et al*. Depleting tumor-specific Tregs at a single site eradicates disseminated tumors. *J Clin Invest* 2013;123:2447–63.
16 Hildner K, Edelson BT, Purtha WE, *et al*. Batf3 deficiency reveals a critical role for CD8alpha+ dendritic cells in cytotoxic T cell immunity. *Science* 2008;322:1097–100.
17 Peggs KS, Quezada SA, Chambers CA, *et al*. Blockade of CTLA-4 on both effector and regulatory T cell compartments contributes to the antitumor activity of anti-CTLA-4 antibodies. *J Exp Med* 2009;206:1717–25.
18 Simpson TR, Li F, Montalvo-Ortiz W, *et al*. Fc-dependent depletion of tumor-infiltrating regulatory T cells co-defines the efficacy of anti-CTLA-4 therapy against melanoma. *J Exp Med* 2013;210:1695–710.
19 Ingram JR, Blomberg OS, Rashidian M, *et al*. Anti-CTLA-4 therapy requires an Fc domain for efficacy. *Proc Natl Acad Sci U S A* 2018;115:3912–7.
20 Veitonmäki N, Hansson M, Zhan F, *et al*. A human ICAM-1 antibody isolated by a function-first approach has potent macrophage-dependent antimyeloma activity in vivo. *Cancer Cell* 2013;23:502–15.
21 Buchan SL, Dou L, Remer M, *et al*. Antibodies to costimulatory receptor 4-1BB enhance anti-tumor immunity via T regulatory cell depletion and promotion of CD8 T cell effector function. *Immunity* 2018;49:958–70.
22 Waterhouse P, Penninger JM, Timms E, *et al*. Lymphoproliferative disorders with early lethality in mice deficient in CTLA-4. *Science* 1995;270:985–8.
23 Fransen MF, van der Sluis TC, Ossendorp F, *et al*. Controlled local delivery of CTLA-4 blocking antibody induces CD8+ T-cell-dependent tumor eradication and decreases risk of toxic side effects. *Clin Cancer Res* 2013;19:5381–9.
24 Bommareddy PK, Shettigar M, Kaufman HL. Integrating oncolytic viruses in combination cancer immunotherapy. *Nat Rev Immunol* 2018;18:498–513.
25 Foloppe J, Kempf J, Futin N, *et al*. The enhanced tumor specificity of TG6002, an armed oncolytic vaccinia virus deleted in two genes involved in nucleotide metabolism. *Mol Ther Oncolytics* 2019;14:1–14.
26 Kleinpeter P, Fend L, Thioudellet C, *et al*. Vectorization in an oncolytic vaccinia virus of an antibody, a Fab and a scFv against programmed cell death -1 (PD-1) allows their intratumoral delivery and an improved tumor-growth inhibition. *Oncoimmunology* 2016;5:e1220467.
27 Fend L, Yamazaki T, Remy C, *et al*. Immune checkpoint blockade, immunogenic chemotherapy or IFN-α blockade boost the local and Abscopal effects of oncolytic virotherapy. *Cancer Res* 2017;77:4146–57.
28 Liu Z, Ravindranathan R, Kalinski P, *et al*. Rational combination of oncolytic vaccinia virus and PD-L1 blockade works synergistically to enhance therapeutic efficacy. *Nat Commun* 2017;8:14754.
29 Marchand J-B, Semmrich M, Fend L. Antibody-armed oncolytic vaccinia virus to block immunosuppressive pathways in the tumor microenvironment. Society of immunotherapy 33rd annual meeting National Harbour, MD. *J Cancer Ther* 2018.
30 Grosso JF, Jure-Kunkel MN. CTLA-4 blockade in tumor models: an overview of preclinical and translational research. *Cancer Immun* 2013;13:5.
31 Andtbacka RHI, Kaufman HL, Collichio F, *et al*. Talimogene Laherparepvec improves durable response rate in patients with advanced melanoma. *J Clin Oncol* 2015;33:2780–8.
32 Chesney J, Puzanov I, Collichio F, *et al*. Randomized, open-label phase II study evaluating the efficacy and safety of Talimogene Laherparepvec in combination with ipilimumab versus ipilimumab alone in patients with advanced, unresectable melanoma. *J Clin Oncol* 2018;36:1658–67.
33 Ngwa W, Irabor OC, Schoenfeld JD, *et al*. Using immunotherapy to boost the abscopal effect. *Nat Rev Cancer* 2018;18:313–22.
34 DiLillo DJ, Ravetch JV. Differential Fc-receptor engagement drives an anti-tumor vaccinal effect. *Cell* 2015;161:1035–45.
35 Gubin MM, Zhang X, Schuster H, *et al*. Checkpoint blockade cancer immunotherapy targets tumour-specific mutant antigens. *Nature* 2014;515:577–81.
36 Nakagawa H, Sido JM, Reyes EE, *et al*. Instability of Helios-deficient Tregs is associated with conversion to a T-effector phenotype and enhanced antitumor immunity. *Proc Natl Acad Sci U S A* 2016;113:6248–53.
37 Hui E, Cheung J, Zhu J, *et al*. T cell costimulatory receptor CD28 is a primary target for PD-1-mediated inhibition. *Science* 2017;355:1428–33.
38 Wei SC, Duffy CR, Allison JP. Fundamental mechanisms of immune checkpoint blockade therapy. *Cancer Discov* 2018;8:1069–86.
39 Simon S, Voillet V, Vignard V, *et al*. PD-1 and TIGIT coexpression identifies a circulating CD8 T cell subset predictive of response to anti-PD-1 therapy. *J Immunother Cancer* 2020;8:e001631.
40 Galletti G, De Simone G, Mazza EMC, *et al*. Two subsets of stem-like $CD8^+$ memory T cell progenitors with distinct fate commitments in humans. *Nat Immunol* 2020;21:1552–62.
41 Galon J, Bruni D. Approaches to treat immune hot, altered and cold tumours with combination immunotherapies. *Nat Rev Drug Discov* 2019;18:197–218.
42 Gutierrez M, Long GV, Friedman CF, *et al*. Anti-CTLA-4 probody BMS-986249 alone or in combination with nivolumab in patients with advanced cancers: initial phase I results. *J Clin Oncol* 2020;38:3058–58.
43 Aroldi F, Sacco J, Harrington K, *et al*. 421 Initial results of a phase 1 trial of RP2, a first in class, enhanced potency, anti-CTLA-4 antibody expressing, oncolytic HSV as single agent and combined with nivolumab in patients with solid tumors. *J ImmunoTherapy Cancer* 2020;8:A447–57.
44 Garris CS, Arlauckas SP, Kohler RH, *et al*. Successful anti-PD-1 cancer immunotherapy requires T Cell-Dendritic cell crosstalk involving the cytokines IFN-γ and IL-12. *Immunity* 2018;49:1148–61.
45 Salmon H, Idoyaga J, Rahman A, *et al*. Expansion and activation of CD103(+) dendritic cell progenitors at the tumor site enhances tumor responses to therapeutic PD-L1 and BRAF inhibition. *Immunity* 2016;44:924–38.
46 Mao T, Song E, Iwasaki A. PD-1 blockade-driven anti-tumor CD8+ T cell immunity requires XCR1+ dendritic cells. *bioRXIV*2021.
47 Solomon I, Amann M, Goubier A, *et al*. CD25-$T_{reg}$-depleting antibodies preserving IL-2 signaling on effector T cells enhance effector activation and antitumor immunity. *Nat Cancer* 2020;1:1153–66.
48 Wei SC, Anang N-AAS, Sharma R, *et al*. Combination anti-CTLA-4 plus anti-PD-1 checkpoint blockade utilizes cellular mechanisms partially distinct from monotherapies. *Proc Natl Acad Sci U S A* 2019;116:22699–709.
49 Ribas A, Camacho LH, Lopez-Berestein G, *et al*. Antitumor activity in melanoma and anti-self responses in a phase I trial with the anti-cytotoxic T lymphocyte-associated antigen 4 monoclonal antibody CP-675,206. *J Clin Oncol* 2005;23:8968–77.
50 Zappasodi R, Serganova I, Cohen IJ, *et al*. CTLA-4 blockade drives loss of $T_{reg}$ stability in glycolysis-low tumours. *Nature* 2021;591:652–8.
51 Kim JM, Rasmussen JP, Rudensky AY. Regulatory T cells prevent catastrophic autoimmunity throughout the lifespan of mice. *Nat Immunol* 2007;8:191–7.
52 Chambers CA, Krummel MF, Boitel B, *et al*. The role of CTLA-4 in the regulation and initiation of T-cell responses. *Immunol Rev* 1996;153:27–46.
53 Leach DR, Krummel MF, Allison JP. Enhancement of antitumor immunity by CTLA-4 blockade. *Science* 1996;271:1734–6.

J Immunother Cancer: first published as 10.1136/jitc-2021-003488 on 19 January 2022. Downloaded from http://jitc.bmj.com/ on April 19, 2024 by guest. Protected by copyright.

**Supplemental information**

# Vectorized Treg-depleting αCTLA-4 elicits antigen cross-presentation and $CD8^+$ T cell immunity to reject "cold" tumors

## Material and Methods

**Cell lines.** Human embryonic kidney cell line 293T, murine melanoma B16-F10, murine colon carcinoma CT26, murine B cell lymphoma A20, murine mammary EMT6 and the murine Lewis lung carcinoma cell line (LL/2) were purchased from the American Type Culture Collection (ATCC) and cells stably transfected with human CTLA-4 (293T-CTLA-4) from Crown Bio. Cells were cultured in RPMI+ glutamax (CT26) or DMEM+ glutamax (MC38, B16-F10, LL/2) supplemented with 10% FCS, 10 mM HEPES and 1 mM sodium pyruvate. EMT6 cells were maintained in Waymouth medium supplemented with 15% FCS, 10 mM HEPES and 1 mM sodium pyruvate. The NK-92 cell line expressing hFcγRIIIA-158V together with GFP (purchased from ATCC) was cultured in supplemented α-MEM medium.[1] Primary cells were cultured in R10 medium (RPMI 1640 containing 2 mM glutamine, 1 mM pyruvate, 100 IU/ml penicillin and streptomycin and 10% FBS; GIBCO by Life Technologies). The human colorectal adenocarcinoma cell line LoVo (ATCC), pancreatic tumor cell line MIA PaCa-2 (ATCC) and human gastric carcinoma cell line Hs-746 T (ATCC) were grown in DMEM (Gibco) supplemented with 10 % FBS and containing gentamicin at 40 mg/L. The human ovarian tumor cell line SK-OV-3 (ATCC) and human colorectal carcinoma cell line HCT 116 (ATCC) were grown in Mc Coy's 5A medium (ATCC) supplemented with 10 % FBS and containing gentamicin at 40 mg/L. The human erythroblast cell line TF-1 (ATCC) was grown in RPMI 1640 (Sigma) supplemented with 10 % FBS and containing gentamicin at 40 mg/L + GM-CSF at 2 ng/mL.

**Antibodies.** Monoclonal antibodies for flow cytometry: Anti-human CD4-VioGreen (M-T466) Miltenyi Biotec Cat# 130-113-259, Anti-human CD25-BV421 (clone M-A251) BD Biosciences Cat# 562442, Anti-human CD127-FITC (clone HIL-7R-M21) BD Biosciences Cat# 561697 , Anti-human CD8-APC (clone RPA-T8) BD Biosciences Cat# 555369, Anti-human CTLA-4-PE (clone BNI3) BD Biosciences Cat# 555853, mouse IgG2a, k isotype control -PE BD Biosciences Cat# 555574, Anti-mouse CD45.2-PerCP-Cy5.5 (clone 104) BD Biosciences Cat# 552950, Anti-mouse CD45.2-BUV737 (clone 104) BD Biosciences Cat# 612779, Anti-mouse CD25-BV421 (clone 7D4) BD Biosciences Cat# 564571, Anti-

mouse CD8-BV786 (clone 53-6.7 ) BD Biosciences Cat# 563332, Anti-mouse CD4 -BV510 (clone RM4-5) BD Biosciences Cat# 563106, Anti-mouse TCRb-Alexa Fluor 488 (clone H57-597) BioLegend Cat# 109215, Anti-mouse PD-1-BB700 (clone RMP1-30) BD Biosciences Cat# 748242, Anti-mouse CTLA-4-PECF594 (clone UC10-4F10-11) BD Biosciences Cat# 564332, Anti-mouse CTLA-4-APC (clone UC10-4B9) BioLegend Cat# 106310, Anti-mouse Klrg1-APC (clone 2F1) BD Biosciences Cat# 561620, Anti-mouse CD62L-BUV395 (clone MEL-14 ) BD Biosciences Cat# 740218, Anti-mouse TIM3-PE (clone 5D12) BD Biosciences Cat# 566346, Anti-mouse ICOS-BV605 (clone 7E.17G9) BD Biosciences Cat# 745254, Anti-mouse CD44-APC-Cy7 (clone IM7) BD Biosciences Cat# 560568, Anti-mouse Ly6C Alexa Fluor 488 (clone HK1.4) BioLegend Cat# 128022, Anti-mouse CD24 PerCP-Cy™5.5 (clone M1/69) BD Biosciences Cat# 562360, Anti-mouse MHC-II BV421 (clone M5/114.15.2) BD Biosciences Cat# 562564, Anti-mouse CD172a (SIRPα) BV510 (clone P84) ) BioLegend Cat# 144032, Anti-mouse CD64 (FcγRI) BV605 (clone X54-5/7.1) ) BioLegend Cat# 139323, Anti-Mouse CD8a BV650 (clone 53-6.7) BioLegend Cat# 563234, Anti-mouse F4/80 BV785 (clone BM8) BioLegend Cat# 123141, Anti-Mouse CD45 BUV395 (clone 30-F11) BD Biosciences Cat# 564279, Anti-mouse/rat XCR1 Alexa Fluor 647 (clone ZET) BioLegend Cat# 148214, Anti-mouse CD103 Alexa Fluor 700 (clone 2E7) BioLegend Cat# 121442, Anti-mouse CD19 PE (clone 1D3) BD Biosciences Cat# 553786, Anti-mouse CD170 (Siglec-F) PE (clone S17007L) BioLegend Cat# 155506, Anti-mouse NK-1.1 PE (clone PK136) BioLegend Cat# 108708, Anti-mouse TCR-β chain PE (clone H57-597) BioLegend Cat# 109208, Anti-mouse CD11c PE/Dazzle™ 594 (clone N418) BioLegend Cat# 117348, Anti-mouse CD11b PE-Cy7 (clone M1/70) BD Biosciences Cat# 552850, Anti-mouse Ki67-Alexa Fluor 700 (clone B56) BD Biosciences Cat# 561277, Anti-human Granzyme B- R718 (clone GB11) BD Biosciences Cat# 566964, Anti-mouse Tbet-BV711 (clone O4-46) BD Biosciences Cat# 563320, Anti-mouse FoxP3-PeCy7 (clone FJK-16s ) Thermo Fisher Scientific Cat# 17-5773-82, Anti-mouse IFNg-PeCy7 (clone XMG1.2) BioLegend Cat# 505826, Anti-mouse TNFa-Alexa Fluor 700 (clone MP6-XT22) BD Biosciences Cat# 558000, Pentamer H-2Ld – SPGAAGYDL-R-PE (S9L8) ProImmune, Pentamer H-2Ld – TPHPARIGL-R-PE (ctrl) ProImmune,

Dextramer H-2Ld – SPSYVYHQF-APC (AH-1) Immudex, Dextramer H-2Ld – TPHPARIGL-APC (ctrl) Immudex.

Secondary antibodies: Goat Anti-Mouse IgG (H+L) Peroxidase Jackson ImmunoResearch Cat# 115-035-003, Goat Anti-Human IgG (H+L) Peroxidase Jackson ImmunoResearch Cat# 109-035-003, Goat Anti-Human IgG, Fc-Fragment Specific- APC Jackson ImmunoResearch Cat# 109-136-098, Goat Anti-Human IgG-APC Jackson ImmunoResearch Cat# 109-136-088, Goat Anti-Human Kappa Light Chain HRP Bethyl Cat# A80-115P, Goat Anti-Mouse Lambda Light Chain HRP Bethyl Cat# A90-121P, Goat Anti-Mouse IgG-APC Jackson ImmunoResearch Cat# 115-136-146, Anti-His MAb, (clone AD1.1.10) R&D Systems Cat# MAB050, Anti-His-HRP (clone AD1.1.10) R&D Systems Cat# MAB050H.

Commercially antibodies used for in vivo experiments: Anti-mouse CD8 (clone 53.6.72) BioXCell Cat# BP0004-1 , Anti-mouse CD4 (clone GK1.5) BioXCell Cat# BE0003-1, Anti-mouse PD1 (clone 29F.1A12) BioXCell Cat# BE0273, Anti-trinitrophenol rIgG2a isotype control (clone 2A3) BioXCell Cat# BE0089, Anti-mouse CTLA-4 (clone 9H10) BioXCell Cat# BE0131, Anti-mouse PD1 (clone RMP1-14) BioXCell Cat# BE0146.

In-house generated anti-mouse and anti-human antibodies isolated from the n-CoDeR phage display library. Anti-mouse CTLA-4 (clone 5-B07) and Anti-human CTLA-4 (clone 4-E03) are described here in this paper.

**Isolation of Treg depleting antibodies specific for tumor Treg-associated receptors.** Antibodies specific for tumor Treg cell-associated receptors were isolated by subjecting the in vitro CDR shuffled n-CoDeR® antibody library to differential biopanning of tumor-associated Treg cells (isolated from CT26, 4T1, B16 and Lewis lung tumor-bearing mice) versus $CD4^+$ T cell-depleted naïve cells and $CD11b^+$ cells from tumor-bearing mice essentially as described previously.[2]

**CTLA-4 mAb Generation.** Antibody fragments against human/mouse CTLA-4 were isolated from the n-CoDeR® scFv phage display library. Enrichment of specific CTLA-4 antibodies was achieved by three

consecutive pannings using biotinylated h/mCTLA-4-His protein (Sino Biological) loaded on Streptavidin Dynabeads or polystyrene balls. The third selection round also included suspension adapted HEK293-EBNA cells transient transfected with cDNA (Sino Biological) encoding the extracellular and transmembrane regions of h/mCTLA-4 or an irrelevant non-target protein. Pre-selection occurred prior to each selection with a biotinylated non-target protein. Binding phages were eluted after each selection round by trypsin digestion and amplified on plates using standard procedures.[3] Phagemids from selection 3 were converted to scFv producing format and used in subsequent screening assays where specific binding to soluble (recombinant protein) and cell bound antigens (transient transfected cells) was assessed. Commercial antibodies were used for the evaluation of recombinant and cell surface bound human (Yervoy, Bristol Myers Squibb; anti-human APC, Jackson) and anti-mouse CTLA-4 (BioLegend) CTLA-4 by flow cytometry, fluorescence microarray technology (FMAT) and ELISA. Corresponding isotype controls were included as negative controls in all experiments. For primary screening of scFv, h/mCTLA-4 transfected cells were seeded into FMAT plates. E. coli expressed scFv were added followed by deglycosylated mouse anti-His antibody (R&D Systems) and anti-mouse-APC (Jackson). Stained cells were detected using the 8200 detection system (Applied Biosystems). Positive clones from the primary screening were re-expressed and re-tested for binding to transfected cells and to recombinant protein in ELISA. For ELISA, E. coli expressed scFv were added to plates coated with h/mCTLA-4 or non-target protein. Bound scFv were detected using anti-FLAG-AP (Sigma Aldrich) followed by substrate addition (CDP-star, Life Technologies) and luminescence reading (Tecan Ultra).

In total 42 and 31 unique clones were converted to hIgG1 and mIgG2a variants, respectively. VH and VL were PCR amplified and inserted into expression vectors containing the heavy- and light-chain constant regions of the antibody, respectively, and transfected into suspension adapted HEK 293EBNA cells (ATCC). Culture media was harvested 6 days post-transfection and antibodies were purified using columns packed with MabSelect (GE Healthcare) connected to an ÄKTA Purifier system, according to standard procedures. Antibodies were eluted with a low-pH buffer and then

dialyzed to an appropriate formulation buffer using a Spectra/Por Dialysis Membrane 4 (Spectrum Laboratories Inc) before a final sterile-filtration.

Antibody purity was assessed by CE-SDS (LabChip XII; Perkin Elmer, Massachusetts, USA) and SE-HPLC (Ultimate 3000, Thermo Fisher Scientific). All preparations were endotoxin low (<0.1 EU/mg protein) as determined using the Chromogenic LAL-Endochrome-K kit (Charles River) adapted to European Pharmacopoeia 2.6.14, current version: Bacterial Endotoxins, "Method D. Chromogenic Kinetic method".

Purified IgG was then assessed for binding to transfected HEK cells as well as primary cells and to recombinant protein, in both ELISA and Biacore.

**Surface Plasmon Resonance.** Binding to recombinant protein was also tested with the surface plasmon resonance (SPR) technology, using Biacore 3000. Anti-human Fc (GE Healthcare) was immobilized on a CM5 sensor chip (GE Healthcare) as a capture antibody with a concentration of 330 nM. Optimal concentrations of 4-E03 and ipilimumab together with the recombinant protein were assessed in pre-tests to obtain good curve fitting and limit mass transfer. Antibodies (5 nM in this particular experiment) were added at 10 µl/min for 1 min, followed by titrating concentrations (1.6 to 50 nM for 4-E03 and 1.6 to 200 nM for ipilimumab) of human CTLA-4 protein (Sino Biological) at 30 µl/min, for 3 min. The surface was regenerated with 10 mM glycine, pH 1.5, between each cycle.

**Cell transfections.** cDNA encoding human and mouse (Sino Biological) CTLA-4 was transfected into suspension adapted 293FT cells (Life Technologies) using Lipofectamine 2000 (Life Technologies). The transfected cells were cultured in FreeStyleTM 293 Expression Medium (Life Technologies) at 37ºC and 5% CO2, 120 rpm for 48h. Target expression was analysed using flow cytometry.

**VV generation and purification.** Recombinant viruses were generated by two successive homologous recombination in chicken embryo fibroblast (CEF) using a starting parental Copenhagen

vaccinia virus encoding GFP or mCherry at J2R and I4L loci and two transfer plasmids. Transfer plasmids encoded either heavy chain of mAb under the p7.5 promoter and flanked by J2R recombination arms, or the light chain of mAb under the p7.5 promoter in addition, or not, of the murine or human GM-CSF under the pSE/L promoter and flanked by I4L recombination arms (see Figure 2A). The recombinant viruses were isolated by several cycles of amplification/isolation of non-fluorescent plaques. Recombinant viruses were then produced on CEF and purified after cells lysis by 5 µm filtration followed by purification/concentration using 0.2 µm tangential flow filtration. Finally, the viruses were formulated in saccharose 50 g/L, NaCl 50 mM, Tris 10 mM, Sodium Glutamate 10 mM, pH 8 by diafiltration, aliquoted and stored at -80 °C until use.

All the viruses used for this publication were from the TK-RR- Copenhagen strain:

VV: unarmed vaccinia virus or TG6002 (vaccinia virus encoding FCU1 chimeric enzyme, benchmark recombinant VV)

$VV_{GM}$: vaccinia virus encoding murine GM-CSF

$VV_{GM}$-αCTLA-4: vaccinia virus encoding murine GM-CSF and 5-B07 (αmouse CTLA-4, mouse IgG2a)

VV-αCTLA-4: vaccinia virus encoding 5-B07

$VV_{GM}$-αhCTLA-4 (BT-001): vaccinia virus encoding human GM-CSF and 4-E03 (αhuman CTLA-4, human IgG1)

**Virus replication, oncolytic activity and transgenes expression in vitro.** Replication of BT-001 was assessed by measuring the total virus titer at 24-, 48- and 72-hours post-infection of LoVo cells with BT-001 at multiplicity of infection (MOI) of $10^{-3}$ (i.e. 1 virus for 1000 cells). Virus titer was determined by plaque assay on Vero cells.

Oncolytic activity of BT-001 was assessed by quantification of cell viability using cell counter (Vi-Cell) after 5 days of incubation of MIA PaCa-2 cells with BT-001 at the MOI indicated in Figure legend.

Both replication and oncolytic activity of BT-001 were benchmarked with those of Copenhagen TK-RR- vaccinia virus TG6002 currently under clinical evaluation.[4]

Transgene expression was assessed after infection by BT-001, at MOI 0.05, of several human tumor cell lines: LoVo, HCT 116 (Colon cancer), MIA PaCa-2 (Pancreatic cancer), SK-OV3 (ovarian cancer) and Hs176T (gastric cancer). Culture supernatants were collected 48 hours post-infection, centrifuged and filtered on 0.2 µm prior measurements of 4-E03 and hGM-CSF concentrations by ELISA.

**Antibody purification from culture medium of BT-001 infected cells.** Fifteen F175 flasks containing ~4.7 $10^7$ MIA PaCa-2 cells/flask were infected at MOI 0.01 with BT-001 in DMEM without bovine serum. Seventy-two hours after infection the cells supernatants were harvested, pooled, centrifuged and filtered on 0.2 µm before adding EDTA (2 mM final) and Tris pH 7.5 (20 mM final). The pool supernatant was loaded, at 4 °C, on a one mL protA Hitrap column (GE healthcare, ref 17-5079-01) previously equilibrated in PBS. The bound antibodies were eluted by 100 mM glycine HCl pH 2.8 and dialyzed against PBS. Purified 4-E03 was loaded on SDS-PAGE (NuPage Bis-Tris gels 4-12% Thermo NP0323) under reducing or non-reducing conditions and the gel was stained with InstantBlue (Expedeon, ISB1L) Coomassie blue. This purified antibody (i.e. 4-E03 MIA PaCa-2) was further assessed for CTLA-4 binding and *in vivo* Treg depletion activity.

**Enzyme-linked immunosorbent assays.**

*GM-CSF.* Human and murine GM-CSF concentrations were determined using the Quantikine®ELISA GM-CSF Immunoassays (R&D Systems).

Human GM-CSF functionality was assessed using the TF-1 proliferation assay. The cellular proliferation of TF-1 cells in presence of known concentrations of hGM-CSF (standard or from BT-001-infected cells) was measured by colorimetry using the enzymatic conversion of MTS to formazan (measured by absorbance at 490 nm) by the dehydrogenases of viable cells. The absorbance at 490 nm was plotted versus the concentration of GM-CSF and the curves compared to the one obtained with recombinant GM-CSF (i.e. Molgramostim).

*Binding to CTLA-4/ CD28 protein.* For antibody binding ELISA, purified human CTLA-4-Fc, human CD28-Fc (R&D Systems) and mouse CTLA-4-Fc (Sino Biologicals) were coated to the assay plate at 1 pmol/well while mouse CD28-His (R&D Systems) was coated at 5 pmol/well. The different antibodies were added at 10 µg/ml and left to bind for 1 h at room temperature. Bound n-CoDeR® mIgG$_{2A}$ or hIgG1 antibodies were detected using either anti-mouse/anti-human H+L-HRP (Jackson Immunoresearch) or anti-mouse/human Lambda Light Chain Antibody HRP (Bethyl). A chromogenic (TMB T0440) or luminescence substrate (Pierce 37070) was used and plate reading was performed with a Tecan Ultra.

*Blocking CD80/CD86 interaction.* For ligand blocking ELISA, purified human CTLA-4-Fc (R&D Systems) was coated to assay plates at 2 pmol/well (for CD80) or 1 pmol/well (for CD86). Antibodies were added at concentrations ranging from 0.4 pM to 67 nM and left to bind for 1 hour. His-tagged ligands were added at 200 nM and 100 nM, respectively (rhCD80 and rhCD86; R&D Systems) as optimized in a pilot experiment by ELISA (data not shown). The plates were further incubated for 15 minutes. After washing, bound ligand was detected with an HRP-labelled anti-His antibody (R&D Systems). Super Signal ELISA Pico (Thermo Scientific) was used as substrate and the plates were analysed using Tecan Ultra Microplate reader. Alternatively, mouse CTLA-4-Fc (Sino Biological) was coated to assay plates at 1 pmol/well. Antibodies were added at a starting concentration of 10 µg/ml (67 nM), with 2-fold dilution steps and left to bind for 1 hour. His-tagged ligands, CD80 and CD86 (Sino Biological), were added at 50 nM and the plates were further incubated for 30 minutes. Detection and reading were performed as described above.

**Processing of human tissue.** Ovarian tumor samples obtained from patients undergoing surgery were cut into small pieces and incubated in R10 with DNase I (Sigma) and Liberase TM (Roche Diagnostics) for 20 min at 37°C. Remaining tissue was mechanically dissociated and, together with the cell suspension, passed through a 70 µm cell strainer. Matched peripheral blood samples were obtained and peripheral blood mononuclear cells were separated using Ficoll-Paque PLUS (Cytiva) by

centrifugation over Leucosep tubes (Greiner) at 800 x *g* for 20 minutes. Human buffy coats were obtained from the blood center in the hospital of Halmstad (Sweden) and processed according to standard protocol.

**Mouse experiments.**

*In vivo tumor experiments.* Cultured tumor cells were injected subcutaneously in the left flank only or both flanks (CT26 $1x10^6$ cells; MC38 $5x10^5$ cells; A20 $5x10^6$ cells; EMT6 $1x10^6$ cells; B16-F10 0.5–$5x10^5$ cells, LL/2 $5x10^5$ cells). Unless otherwise specified, mice were treated i.t. with $10^7$ pfu of $VV_{GM}$-αCTLA-4 or control VV, thrice, every other day. For tumor growth experiments, tumor sizes of treated and distant tumors were measured twice a week with a caliper and tumor volume ($mm^3$) was calculated according to the formula: ($width^2$× length × 0.52). Animals were euthanized when the total tumor burden (treated and contralateral tumors combined) reached a volume of 2000 $mm^3$ (experimental endpoint). For functional experiments, tissues were collected and processed at the time points indicated in Figure legends. Mouse tumors were digested in R10 with DNase I (Sigma) and Liberase TM (Roche Diagnostics) for 15 mins at 37°C. Cells were then passed through a 70 μm cell strainer and used for assays directly. For DC phenotyping, viable leucocytes were enriched following density gradient centrifugation (Cedarline Cat#CL5035).

*Primary human xenograft model.* PBMC-NOG/SCID mice were generated by intravenously injecting NOG mice (NOD.Cg-*Prkdc*$^{scid}$ *Il2rg*$^{tm1Sug}$/JicTac (Taconic)) with 1-$2x10^7$ PBMC isolated using Ficoll-Paque PLUS, in 200 µl PBS. Approximately two weeks after injection, SCID mice (C.B-*Igh-1*$^b$/IcrTac-*Prkdc*$^{scid}$ (Taconic)) were subsequently intraperitoneally injected with $10x10^6$ splenocytes from reconstituted NOG mice. 1h later, mice were treated with 10 mg/kg of mAb. The intraperitoneal fluid of the mice was collected after 24 h. Human T cell subsets were identified and quantified by FACS using following markers: CD45, CD4, CD8, CD25, CD127 (all from BD Biosciences).

*Pharmakokinetics of transgenes and virus in tumor and blood.* In CT26 tumor model described previously, $VV_{GM}$-αCTLA-4 or VV-αCTLA-4 were administrated in same conditions as mentioned

above (i.e. 3 i.t. injections of $10^7$ pfu at day 0, 2 and 4). Tumor and blood of three mice/timepoint were collected at day 1, 4 (prior third injection), 8 and 10. Concentrations of virus were measured in whole blood and in tumor homogenized in PBS by viral titration on Vero cells. Concentrations of both 5-B07 and mGM-CSF were measured by ELISA in serum and tumor homogenates.
In xenografted human tumor model, LoVo cells were injected subcutaneously in the left flank of Swiss nude mice. After about two weeks when the tumor volume reached ~120 $mm^3$ the mice were randomized and split in 2 groups (15 mice/groups). First group was injected once i.t. with $10^5$ pfu of $VV_{GM}$-αhCTLA-4 (BT-001) and second group was injected intraperitoneally with 3 mg/kg of 4-E03. Tumor and blood/serum of three mice/timepoint were collected at day 1, 3, 6, 10 and 20 post-virus injection. The virus titer and concentrations of both 4-E03 and hGM-CSF were measured as described in the previous paragraph.

**Flow cytometry.** Antibodies and fluorescent labels used for staining are listed above. Dead cells were routinely identified using the Fixable Viability Dye eFluor™ 780, the Fixable Viability Stain 440UV or propidium iodide and excluded from the analysis along with doublets. Intracellular staining was performed using the FoxP3 Staining Buffer Set (Thermo Fisher Scientific). Sample acquisition was performed on either a BD FACS Verse or Fortessa-X20 and the data were analyzed using FlowJo 10.7.2. To generate the UMAP of intratumoral and splenic $CD3^+$ T cells, data were cleaned using the FlowAI tool (v.2.2), samples were then barcoded with treatment group and organ, and concatenated. The FlowJo plugin UMAP (v3.1) was run on the resulting flow cytometry standard (FCS) file using the default settings (distance function: Euclidean, nearest neighbors: 15, and minimum distance: 0.5) and including all the compensated parameters and forward scatter (FSC) and side scatter (SSC) measurements. For cluster identification, the FlowJo plugin x-shift (v1.3) was run on the resulting UMAP using the default settings (nearest neighbors $K$ = 82) and including the following parameters: CD4, CD62L, CD25, ICOS, FoxP3, Klrg1, CD44, CTLA-4, PD-1, TIM-3, T-bet, GzmB, Ki-67. Mean expression per cluster for the aforementioned parameters was calculated using

scaled channel values obtained from FlowJo. Mean expression heatmaps were generated with parameter means per cluster and scaled between 0 and 1. For DC analysis, cells were gated on alive $CD45^{+}$, $CD11c^{high}$ $Lineage^{-}$ (TCR-β, CD19, NK1.1, SiglecF), $Ly6C^{low/int}$, $F4/80^{-}$ $CD64^{low}$, $MHC\text{-}II^{high}$ and $CD103^{+}$ $Sirp\alpha^{-}$.

**Antibody Dependent Cellular Cytotoxicity**. ADCC assays were performed using a NK-92 cell line stably transfected to express the CD16-158V allele together with GFP. $CD4^{+}$ target T cells were isolated from peripheral blood of healthy donors using $CD4^{+}$ T cell isolation kit (Miltenyi Biotec). Cells were stimulated for 72 hours with CD3/CD28 dynabeads (Life Technologies, Thermo Fisher) to upregulate CTLA-4 and 50 ng/ml recombinant hIL-2 (R&D Systems) at 37°C. Target cells were pre-incubated with mAb at 10 µg/ml for 30 min at 4°C prior to mixing with NK cells. The cells were incubated for 4h at a 2:1 effector:target cell ratio. Lysis was determined by flow cytometry. Briefly, at the end of the incubation, the cell suspension was stained with VioGreen-conjugated aCD4 (M-T466, Miltenyi Biotec) together with Fixable Viability Dye eFluor780 (eBioscience) for 30 min in the dark at 4°C and the cells were then analysed by FACS.

**Functional block in vitro.** For the SEB PBMC assay, total PBMCs from healthy donors were seeded on 96-well plates ($1x10^5$ cells/well) and stimulated with 1 µg/ml Staphylococcus enterotoxin B (SEB, Sigma Aldrich) in the presence of titrated doses of αCTLA-4 IgGs, ranging from 20-0,625 µg/ml. After 3 days, supernatants were harvested and IL-2 quantified by MSD (Meso Scale Discovery, Rockville, USA) according to manufacturer's instructions.

**In vitro binding assays.** CTLA-4 expressing transfected cells were incubated with the concentrations of αCTLA-4 mAb indicated at 4°C for 20 mins prior to washing and staining with an APC-labelled goat anti-human secondary antibody (Jackson ImmunoResearch). No binding was observed to cells transfected with empty vector (not shown).

IgG binding to primary cells was analyzed on isolated, *in vitro*-activated $CD4^+$ T cells. Briefly, human peripheral $CD4^+$ T-cells were purified from total PBMCs by negative selection using MACS CD4 T-cell isolation kit (Miltenyi Biotec). $CD4^+$ T cells were activated *in vitro* with CD3/CD28 dynabeads (Life Technologies) plus 50 ng/ml recombinant hIL-2 (R&D Systems) in R10 medium for 3 days to upregulate CTLA-4 expression. *In vitro*-activated human $CD4^+$ T cells were incubated with the indicated concentrations of αCTLA-4 mAb together with αCD4. Bound αCTLA-4 mAb were detected with APC-labelled goat-anti-human IgG.

In competitive binding assays, 2 µg/ml Alexa 647-labelled αCTLA-4 mAb was mixed with recombinant human or cynomolgus CTLA-4-Fc protein (50 µg/ml; R&D Systems) prior to incubation with CTLA-4 expressing cells. Bound IgG binding was detected by FACS.

**Antigen-specific T cell responses.** Antigen-specific T cell responses were analyzed in spleen, treated and contralateral tumors. Briefly, 1 x $10^6$ isolated cells were restimulated with 2 µg/ml of tumor (AH-1, SPSYVYHQF)- or virus (S9L8, SPGAAGYDL)- specific peptides (BioNordika).[5 6] Tumor cells were pulsed for 4h in the presence of brefeldin A (Sigma). Isolated splenocytes were restimulated for 48h, the last 4h in the presence of brefeldin A. Cytokine-producing $CD8^+$ T cells were then identified by FACS staining for CD45, TCR-β, CD8, TNF-α, IFN-γ and CD25. In parallel, tumor and virus-specific $CD8^+$ T cells were identified using MHC class I multimers (Pentamer H-2Ld – SPGAAGYDL-R-PE (S9L8) ProImmune, Pentamer H-2Ld – TPHPARIGL-R-PE (ctrl) ProImmune, Dextramer H-2Ld – SPSYVYHQF-APC (AH-1) Immudex, Dextramer H-2Ld – TPHPARIGL-APC (ctrl) Immudex).

**RNA sequencing.**

*Experimental procedure.* CT26 tumor cells were implanted in 10 BALB/c mice per group. Approximately 1 week after implantation when the tumor volume reached 20-50 $mm^3$ (defined as day 0) the mice were non-treated or treated twice, at D0 and D2, by $10^7$ pfu in 50 µL i.t. with either unarmed vaccinia virus (VV empty) or $VV_{GM}$-αCTLA-4. At D4 the tumors were harvested and RNA

extracted using the Qiagen kitRNeasy Plus Mini Kit. The samples were conserved at -80°C till the day of assessment of their quality subsequently. The quality of the purified RNAs was evaluated using Agilent RNA 6000 Nano Kit, Agilent 2100 Bioanalyzer System, 2100 Expert Software to ensure that at least 25 % of the RNA fragments were longer than 200 nt (DV200 > 25 %) as required for subsequent 3' mRNA sequencing. Strand specific libraries were prepared and both ends were sequenced (paired-end sequencing) by IntegraGen, (France) yielding pairs of 100 nt long reads.

*Data analysis.* Paired reads were processed by a custom bioinformatic pipeline. Briefly, unique molecular identifier (UMI) sequence was extracted from read 1 while the sequence of the 3' end of the RNA fragment captured was extracted from read 2. After quality-based trimming and quality control, read 2 were mapped with STAR [7] against a custom genome containing *Mus musculus* full genome (mm10 assembly) plus $VV_{GM}$-αCTLA-4 genome as an artificial extra-chromosome. Reads were then deduplicated using the program dedup from the suit of tools UMI tools [8] with the method "unique". Finally, deduplicated reads were quantified using HTSeq-count.[9] Readcount data per sample was then normalized using DESeq2 [10] and a gene was considered differentially expressed if the fold change between two conditions was above 2, and the adjusted p-value below 0.1 (Benjamini-Hochberg correction for multiple testing). Gene Ontology enrichment analyses were performed using the set of genes differentially expressed as defined above, either up or down-regulated, with the function enrichGO from the R package clusterProfiler.[11]

**Supplemental Figure 1**

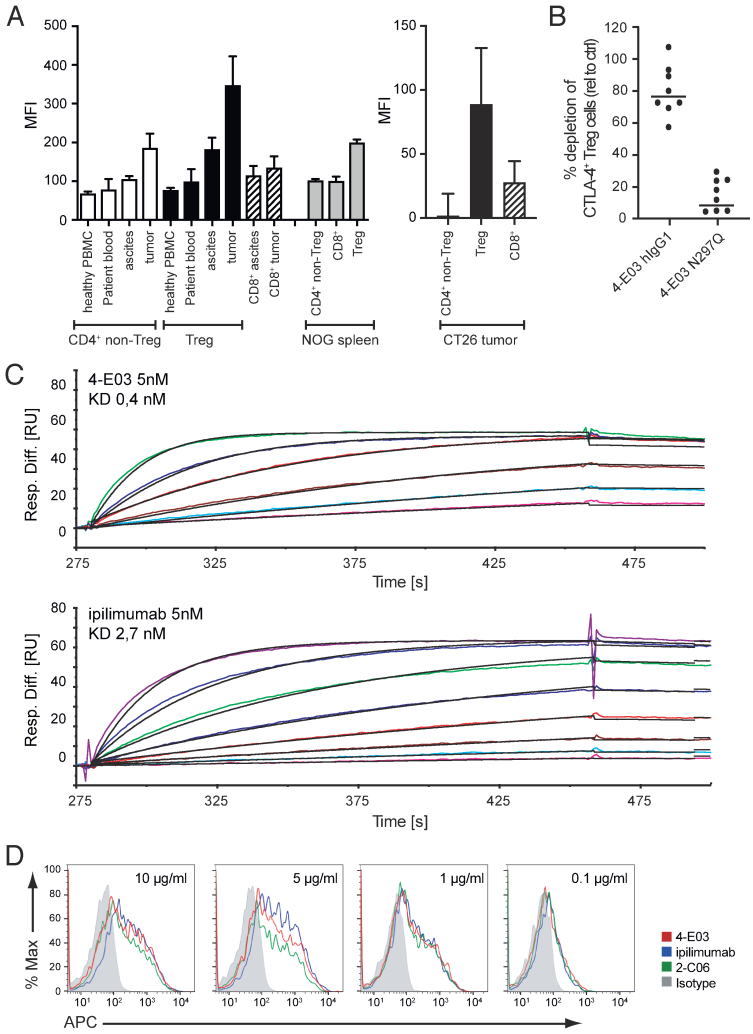


**Supplemental Figure 1 related to Figure 1.** Characterization of hCTLA-4-specific mAbs. (A) Samples of freshly excised ovarian tumors, ascites, and blood were compared to healthy PBMCs. CTLA-4 expression was assessed on $CD4^+$ $CD25^+$ $CD127^-$ Treg cells, $CD4^+$ non-Treg cells, and $CD8^+$ effector T cells by flow cytometry and compared to expression on human T cells isolated from NOG spleens two weeks after PBMC transfer and to CTLA-4 expression on intratumoral T cells from CT26 tumor-bearing mice. Data represent individual patients/ donors with n= 11 for healthy PBMCs, n= 20 for ascites, n= 9 for tumor, and n= 5 for patient blood. (B) Human PBMCs were injected i.v. into NOG mice. 2-3 weeks post transplant, spleens were dissected out and cell suspension was injected i.p. into SCID recipients subsequently treated with 10 mg/kg 4-E03 hIgG1, 4-E03 hIgG1 N297Q or isotype control. Cells were collected by i.p. lavage and quantified 24h post treatment. % cell depletion was normalized to isotype control. Each dot represents one mouse. (C) Binding kinetics of 4-E03 and ipilimumab to soluble human CTLA-4 were evaluated by Biacore analysis. mAbs were captured on the chip by immobilized anti-human Fc and different concentrations of CTLA-4 protein were injected in each cycle. KD values for 4-E03 and ipilimumab were 0.6 nM and 2.7 nM, respectively. (D) Dose-dependent binding of αCTLA-4 mAb to CTLA-4 endogenously expressing human T cells by flow-cytometry.

**Supplemental Figure 2**

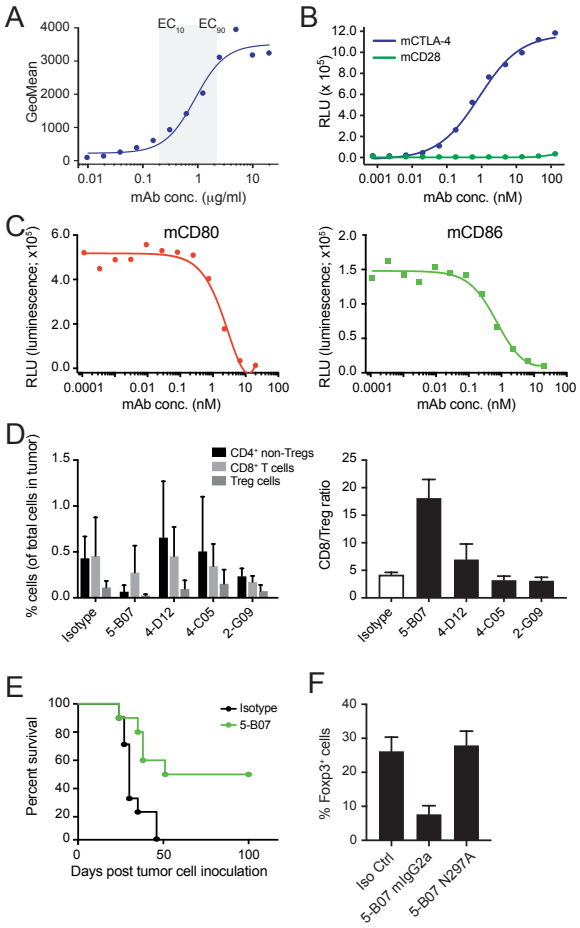


**Supplemental Figure 2 related to Figure 1.** Characterization of mCTLA-4-specific mAbs. (A) Dose-dependent binding of mouse αCTLA-4 mAb to mCTLA-4-transfected cells by flow-cytometry. (B) Binding of titrated doses of mouse surrogate antibody 5-B07 mIgG2a (from 10 µg/ml, with 3-fold dilution steps) was tested against mouse CTLA-4 and CD28 by ELISA. (C) Anti-CTLA-4 mAbs block B7 ligand (CD80 and CD86) binding to recombinant CTLA-4 by ELISA. (D-F) $1x10^6$ CT26 cells were injected s.c. into BALB/c mice. When tumors reached a size of approximately 100 $mm^3$, mice received 200 µg (10 mg/kg) of CTLA-4-specific mAbs or isotype control antibody on days 0, 4 and 7. (D) Treg depleting activity and $CD8^+$ T cell/ Treg ratios (n=4-8) at day 8 and (E) survival induced by αmouse CTLA-4 antibodies are shown. (F) Mice received 200 µg (10 mg/kg) of 5-B07 mIgG2a, 5-B07 mIgG1 N297A or isotype control antibody. At day 8, tumors were taken out and TIL analysed by FACS. Data shown are mean values (+SD) of one representative experiment with n=7 mice per group.

**Supplemental Figure 3**

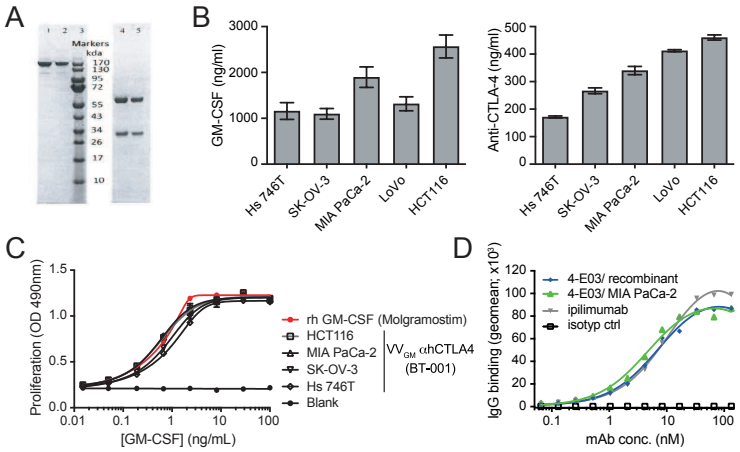


**Supplemental Figure 3 related to Figure 1.** Generation and characterization of oncolytic Vaccinia viruses expressing Treg-depleting αCTLA-4 and GM-CSF. (A) Electrophoresis profile after Coomassie blue staining of 4-E03 purified from MIA PaCa-2 BT-001- infected cell cultures. Lanes 2 and 5: recombinant 4-E03; lanes 1 and 4: 4-E03 purified from culture medium of MIA PaCa-2 BT-001-infected cells. Lanes 1 and 2: non-reducing conditions; Lanes 3 and 4: reducing conditions. (B) Expression levels of 4-E03 and human GM-CSF of indicated human tumor cells 48h post- infection by $VV_{GM}$-αhCTLA-4 (BT-001). (C) Biological activity of GM-CSF produced in E) determined by TF-1 proliferation assay. Recombinant human GM-CSF (Molgramostim obtained from European Pharmacopoeia Reference Standard) was included as positive control. (D) Functional assessment of 4-E03 produced by BT-001-infected MIA PaCa-2 cells by binding to immobilized recombinant hCTLA protein as in Figure 1E.

**Supplemental Figure 4**

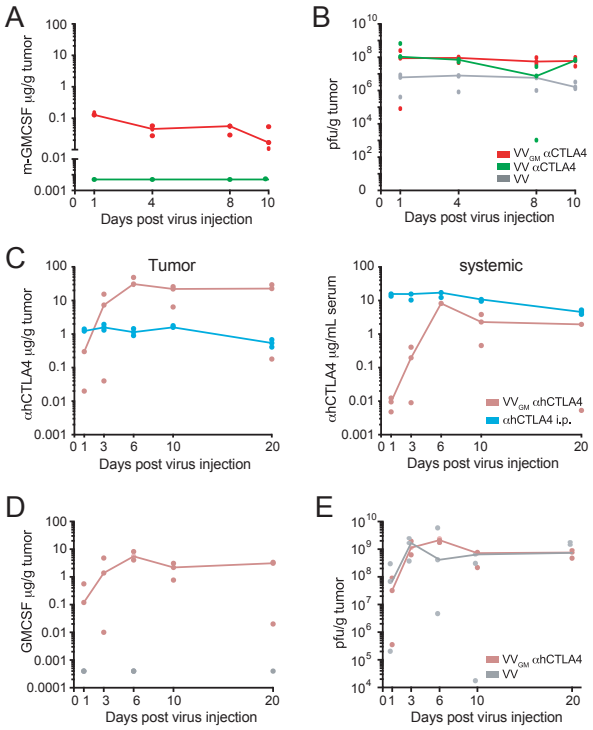


**Supplemental Figure 4 related to Figure 2.** Pharmacokinetics of virus and transgenes in tumor and blood. (A and B) Tumor samples described in Figure 2B were also used to measure the intratumoral concentration of (A) murine GM-CSF and (B) virus load. (C-E) Pharmacokinetics in LoVo xenografted tumor. LoVo cells were implanted in the right flank of Swiss nude mice. When tumor volumes reached ~120 $mm^3$ (defined as D0) mice were treated by a single injection of either $10^5$ pfu of $VV_{GM}$-hCTLA-4 (BT-001) or VV i.t. or 3 mg/kg of 4-E03 monoclonal antibody i.p. Blood and tumors of three mice were collected at each indicated time point. The concentrations of (C) 4-E03, (D) GM-CSF and (E) virus were determined by ELISA and titration on Vero cell, respectively. Lines link the median of values of each time point.

**Supplemental Figure 5**

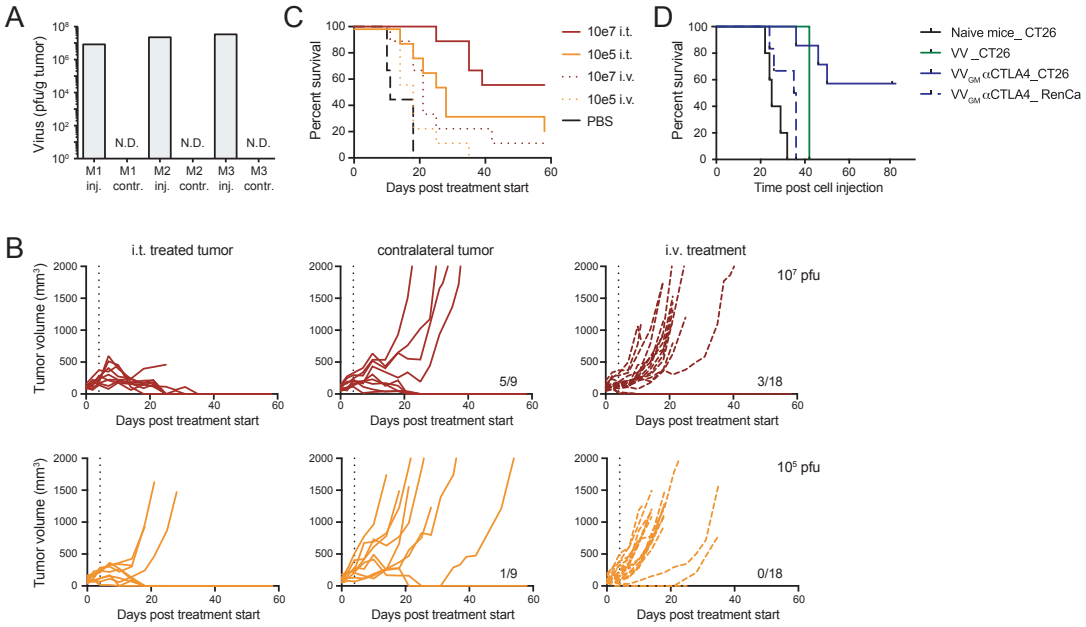


**Supplemental Figure 5 related to Figure 3B.** Treatment with i.t. $VV_{GM}$-αCTLA-4 induces long-lasting anti-tumor responses in treated and untreated tumors. (A) CT26 tumor cells were implanted into the right and left flanks of BALB/c mice. I.t. injections (x3, two days apart) in right flank tumors with $VV_{GM}$-αCTLA-4 started when tumors reached a volume of ~100 $mm^3$. Virus concentration in treated and contralateral tumors was assessed one day post treatment. (n=3 mice per group; mouse 1-3 (M1-3); N.D. = not detected) (B and C) CT26 tumor-bearing mice were treated with indicated doses of $VV_{GM}$-αCTLA-4 as in A). Alternatively, $10^7$ or $10^5$ pfu of $VV_{GM}$-αCTLA-4 was given i.v. Individual tumor growth curves (B) and survival curves (C) are shown. (D) Inhibition of rechallenged tumor growth. CT26 tumor cells were implanted s.c. to BALB/c mice. I.t. treatment with $VV_{GM}$-αCTLA-4 or empty control VV was scheduled as in A). As indicated in the figure legend, surviving mice were s.c. rechallenged with CT26 or Renca cells 100 days after the last VV injection.

**Supplemental Figure 6**

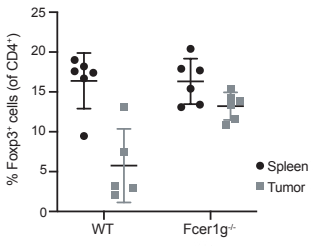


**Supplemental Figure 6 related to Figure 5.** Intratumoral induced $CD8^+$ T cell immunity is FcγR-dependent. WT and *Fcer1g*$^{-/-}$ BALB/c mice were challenged with 1 x $10^6$ CT26 cells s.c. When tumors reached approximately 100 $mm^3$, mice received three i.t. injections of $VV_{GM}$-αCTLA-4 or PBS control at day 0, 2 and 5 ($10^7$ pfu final dose). At day 8, tumors and spleen were isolated and $FoxP3^+$ $CD4^+$ cells analysed by FACS.

**Supplemental Figure 7**

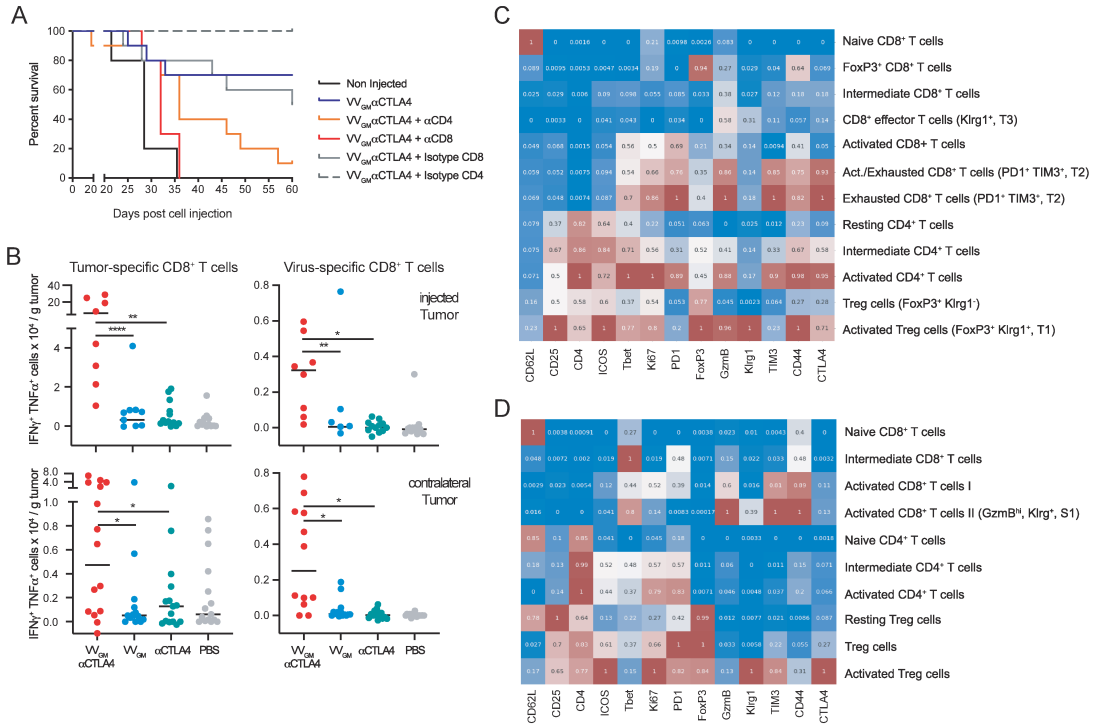


**Supplemental Figure 7 related to Figure 4 and 6.** Treatment with i.t. $VV_{GM}$-αCTLA-4 is dependent on $CD8^+$ T cells. (A) Groups of 10 BALB/c mice were treated, or not, with 1 mg of a CD8- or CD4-depleting antibody (or corresponding isotype control antibodies) 3 days before challenging the mice with 1 x $10^6$ CT26 cells s.c. Another 4 days later (on day -3 relative to treatment start), 200 µg of the depleting antibodies were administered i.p. Mice were then treated i.t. with $VV_{GM}$-αCTLA-4 on days 0, 2 and 4 at 1 x $10^7$ pfu. Percentage survival to the humane end-point is shown. Data are representative for 2 independent experiments. (B) CT26 tumor-bearing mice were treated i.t. with VVs or i.p. with αCTLA-4 mAb (clone 5-B07 at 3 mg/kg). Tumor cell suspensions were restimulated *ex vivo* with VV- or CT26 (AH-1) -specific peptide, cultured for 4h and the number of IFN-$\gamma^+$ and TNFα$^+$ $CD8^+$ T cells was quantified by flow-cytometry. Each dot represents one mouse. Representative experiment (n=3-6) *p < 0.05, **p < 0.01, ****p < 0.0001 by one-way ANOVA. (C and D) Heatmap displaying median marker expression of (C) 12 intratumoral (D) 10 splenic $CD3^+$ subpopulations identified by unsupervised clustering.

**Supplemental Figure 8**

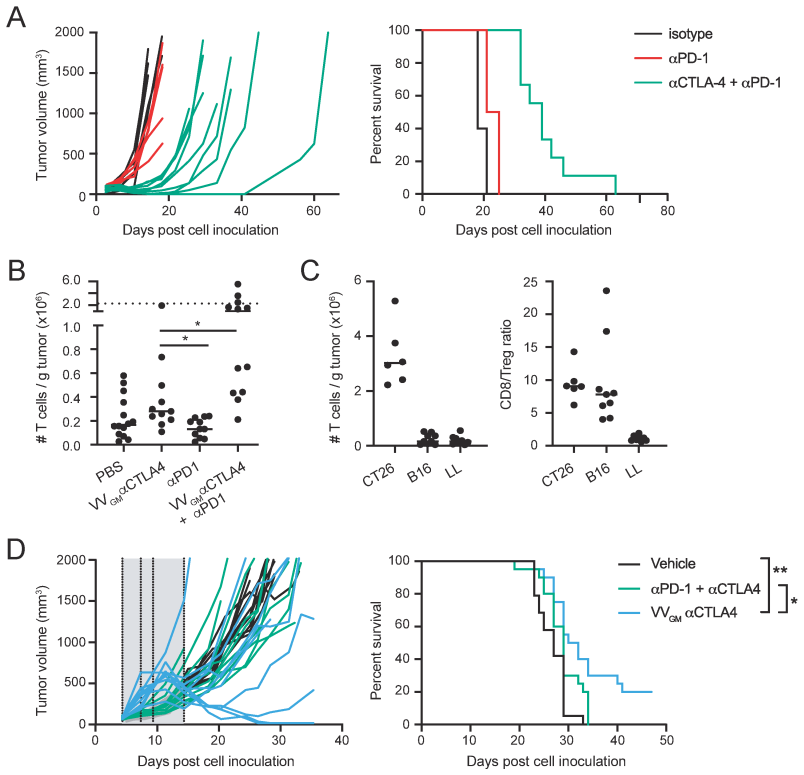


**Supplemental Figure 8 related to Figure 7. Cold B16 and Lewis Lung tumors are refractory to systemic treatment with αCTLA-4 plus αPD-1 but respond to i.t. $VV_{GM}$-αCTLA-4.** (A) B16 tumor-bearing C57BL/6 mice were treated i.p. with αPD-1 at 10 mg/kg or the combination of αPD-1 and αCTLA-4 (10 mg/kg) at day 4, 7, 11. (A) Data are expressed as tumor volume ($mm^3$) on the days after cell inoculation as indicated; each line represents an individual mouse. Panel on the right shows percentage survival to the humane end-point of B16 bearing mice following indicated treatments. (B) B16 tumor-bearing C57BL/6 mice received three i.t. injections with $VV_{GM}$-αCTLA-4 and/or i.p. αPD-1 as described in Figure 7. Six days after the last treatment, tumors were collected and the number of tumor-infiltrating T cells was analyzed by flow cytometry. Each dot represents one mouse. (n=3 experiments). Dotted line indicates number of T cells in the highly T cell inflamed CT26 tumor microenvironment for reference (see also supplemental figure 8C). *$p < 0.05$ by one-way ANOVA. (C) The level of T cell infiltration and $CD8^+$ T cell/ Treg ratios was determined in CT26, Lewis Lung, Renca and 4T1 tumors around day 20 post cell inoculation. (D) Lewis Lung tumor-bearing C57BL/6 mice (tumor start size 50-100 $mm^3$) received four i.t. injections with $VV_{GM}$-αCTLA-4 (vertical dotted lines) or i.p. αPD-1 (10 mg/kg) in combination with αCTLA-4 (3 mg/kg) (twice a week for two weeks, grey area). Tumor growth curves from one representative experiment out of 2 are shown to the left. Corresponding survival (n=20 mice/group, pooled from 2 experiments) is shown in the right panel. *$p < 0.05$, **$p < 0.01$ by Log-rank test.

**Supplemental References**

1. Binyamin L, Alpaugh RK, Hughes TL, et al. Blocking NK cell inhibitory self-recognition promotes antibody-dependent cellular cytotoxicity in a model of anti-lymphoma therapy. *J Immunol* 2008;180(9):6392-401. doi: 10.4049/jimmunol.180.9.6392 [published Online First: 2008/04/22]
2. Veitonmaki N, Hansson M, Zhan F, et al. A human ICAM-1 antibody isolated by a function-first approach has potent macrophage-dependent antimyeloma activity in vivo. *Cancer Cell* 2013;23(4):502-15. doi: 10.1016/j.ccr.2013.02.026 [published Online First: 2013/04/20]
3. Chen T, Hoffmann K, Ostman S, et al. Identification of gliadin-binding peptides by phage display. *BMC Biotechnol* 2011;11:16. doi: 10.1186/1472-6750-11-16 [published Online First: 2011/02/19]
4. Foloppe J, Kempf J, Futin N, et al. The Enhanced Tumor Specificity of TG6002, an Armed Oncolytic Vaccinia Virus Deleted in Two Genes Involved in Nucleotide Metabolism. *Mol Ther Oncolytics* 2019;14:1-14. doi: 10.1016/j.omto.2019.03.005 [published Online First: 2019/04/24]
5. Huang AY, Gulden PH, Woods AS, et al. The immunodominant major histocompatibility complex class I-restricted antigen of a murine colon tumor derives from an endogenous retroviral gene product. *Proc Natl Acad Sci U S A* 1996;93(18):9730-5. doi: 10.1073/pnas.93.18.9730 [published Online First: 1996/09/03]
6. Russell TA, Tscharke DC. Strikingly poor CD8+ T-cell immunogenicity of vaccinia virus strain MVA in BALB/c mice. *Immunol Cell Biol* 2014;92(5):466-9. doi: 10.1038/icb.2014.10 [published Online First: 2014/02/26]
7. Dobin A, Davis CA, Schlesinger F, et al. STAR: ultrafast universal RNA-seq aligner. *Bioinformatics* 2013;29(1):15-21. doi: 10.1093/bioinformatics/bts635 [published Online First: 2012/10/30]
8. Smith T, Heger A, Sudbery I. UMI-tools: modeling sequencing errors in Unique Molecular Identifiers to improve quantification accuracy. *Genome Res* 2017;27(3):491-99. doi: 10.1101/gr.209601.116 [published Online First: 2017/01/20]
9. Anders S, Pyl PT, Huber W. HTSeq--a Python framework to work with high-throughput sequencing data. *Bioinformatics* 2015;31(2):166-9. doi: 10.1093/bioinformatics/btu638 [published Online First: 2014/09/28]
10. Love MI, Huber W, Anders S. Moderated estimation of fold change and dispersion for RNA-seq data with DESeq2. *Genome Biol* 2014;15(12):550. doi: 10.1186/s13059-014-0550-8 [published Online First: 2014/12/18]
11. Yu G, Wang LG, Han Y, et al. clusterProfiler: an R package for comparing biological themes among gene clusters. *OMICS* 2012;16(5):284-7. doi: 10.1089/omi.2011.0118 [published Online First: 2012/03/30]